Electroreduction of nitrate and carbon dioxide on copper electrodes: a mechanistic study

Perez Gallent, E.

References

1. Zumft, W. G., Cell biology and molecular basis of denitrification. *Microbiology and molecular biology reviews* **1997,** *61* (4), 533-616.
2. O'Brien, T. F.; Bommaraju, T. V.; Hine, F., *Handbook of Chlor-Alkali Technology: Volume I: Fundamentals, Volume II: Brine Treatment and Cell Operation, Volume III: Facility Design and Product Handling, Volume IV: Operations, Volume V: Corrosion, Environmental Issues, and Future Developments*. Springer Science & Business Media: 2007; Vol. 1.
3. Gluszcz, P.; Fürch, K.; Ledakowicz, S., Mercury in the chlor-alkali electrolysis industry. In *Bioremediation of Mercury: Current Research and Industrial Applications*, Caister Academic Press Norfolk, UK: 2013; pp 97-118.
4. Grjotheim, K.; Krohn, C.; Malinovsky, M.; Matiasovsky, K.; Thonstad, J., Aluminium electrolysis. Fundamentals of hall-Heroult process. 2-nd edition. *J. Thonstad. Düsseldorf: Aluminium-Verlag* **1982**.
5. Sequeira, C.; Santos, D., Electrochemical routes for industrial synthesis. *Journal of the Brazilian Chemical Society* **2009,** *20* (3), 387-406.
6. Beck, F., Electrosynthesis of adiponitrile in undivided cells. *J. Appl. Electrochem.* **1972,** *2* (1), 59-69.
7. Ding, H.; DeRoy, P. L.; Perreault, C.; Larivée, A.; Siddiqui, A.; Caldwell, C. G.; Harran, S.; Harran, P. G., Electrolytic Macrocyclizations: Scalable Synthesis of a Diazonamide-Based Drug Development Candidate. *Angew. Chem. Int. Ed.* **2015,** *54* (16), 4818-4822.
8. Burgett, A. W.; Li, Q.; Wei, Q.; Harran, P. G., A Concise and Flexible Total Synthesis of (−) ‐ Diazonamide A. *Angew. Chem.* **2003,** *115* (40), 5111-5116.
9. Kita, Y.; Tohma, H.; Kikuchi, K.; Inagaki, M.; Yakura, T., Hypervalent iodine oxidation of N-acyltyramines: synthesis of quinol ethers, spirohexadienones, and hexahydroindol-6-ones. *The Journal of Organic Chemistry* **1991,** *56* (1), 435-438.
10. Martínez-Huitle, C. A.; Rodrigo, M. A.; Sirés, I.; Scialdone, O., Single and Coupled Electrochemical Processes and Reactors for the Abatement of Organic Water Pollutants: A Critical Review. *Chem. Rev.* **2015,** *115* (24), 13362-13407.
11. Ghernaout, D.; Naceur, M. W.; Aouabed, A., On the dependence of chlorine by-products generated species formation of the electrode material

and applied charge during electrochemical water treatment. *Desalination* **2011,** *270* (1), 9-22.
12. Moorcroft, M. J.; Davis, J.; Compton, R. G., Detection and determination of nitrate and nitrite: a review. *Talanta* **2001,** *54* (5), 785-803.
13. Reyter, D.; Chamoulaud, G.; Bélanger, D.; Roué, L., Electrocatalytic reduction of nitrate on copper electrodes prepared by high-energy ball milling. *J. Electroanal. Chem.* **2006,** *596* (1), 13-24.
14. Carpenter, S. R.; Caraco, N. F.; Correll, D. L.; Howarth, R. W.; Sharpley, A. N.; Smith, V. H., Nonpoint pollution of surface waters with phosphorus and nitrogen. *Ecological applications* **1998,** *8* (3), 559-568.
15. Lee, Y. W.; Dahab, M. F.; Bogardi, I., Nitrate risk management under uncertainty. *Journal of Water Resources Planning and Management* **1992,** *118* (2), 151-165.
16. Galloway, J. N.; Schlesinger, W. H.; Levy, H.; Michaels, A.; Schnoor, J. L., Nitrogen fixation: Anthropogenic enhancement-environmental response. *Global Biogeochemical Cycles* **1995,** *9* (2), 235-252.
17. Adam, J., Health aspects of nitrate in drinking-water and possible means of denitrification (literature review). *Water SA* **1980,** *6* (2), 79-89.
18. Wakida, F. T.; Lerner, D. N., Non-agricultural sources of groundwater nitrate: a review and case study. *Water research* **2005,** *39* (1), 3-16.
19. Mani, K., Electrodialysis water splitting technology. *Journal of membrane science* **1991,** *58* (2), 117-138.
20. Panyor, L.; Fabiani, C., Anion rejection in a nitrate highly rejecting reverse osmosis thin-film composite membrane. *Desalination* **1996,** *104* (3), 165-174.
21. Schoeman, J.; Steyn, A., Nitrate removal with reverse osmosis in a rural area in South Africa. *Desalination* **2003,** *155* (1), 15-26.
22. Matějů, V.; Čižinská, S.; Krejčí, J.; Janoch, T., Biological water denitrification—a review. *Enzyme and Microbial Technology* **1992,** *14* (3), 170-183.
23. Duca, M.; Koper, M. T., Powering denitrification: the perspectives of electrocatalytic nitrate reduction. *Energy Environ. Sci.* **2012,** *5* (12), 9726-9742.
24. Rosca, V.; Duca, M.; de Groot, M. T.; Koper, M. T., Nitrogen cycle electrocatalysis. *Chem. Rev.* **2009,** *109* (6), 2209-2244.
25. Da Cunha, M.; De Souza, J.; Nart, F., Reaction Pathways for Reduction of Nitrate Ions on Platinum, Rhodium, and Platinum− Rhodium Alloy Electrodes. *Langmuir* **2000,** *16* (2), 771-777.

26. De Groot, M.; Koper, M., The influence of nitrate concentration and acidity on the electrocatalytic reduction of nitrate on platinum. *J. Electroanal. Chem.* **2004,** *562* (1), 81-94.
27. Tucker, P. M.; Waite, M. J.; Hayden, B. E., Electrocatalytic reduction of nitrate on activated rhodium electrode surfaces. *J. Appl. Electrochem.* **2004,** *34* (8), 781-796.
28. Li, M.; Feng, C.; Zhang, Z.; Sugiura, N., Efficient electrochemical reduction of nitrate to nitrogen using Ti/IrO 2–Pt anode and different cathodes. *Electrochim. Acta* **2009,** *54* (20), 4600-4606.
29. Pletcher, D.; Poorabedi, Z., The reduction of nitrate at a copper cathode in aqueous acid. *Electrochim. Acta* **1979,** *24* (12), 1253-1256.
30. Dima, G.; Beltramo, G.; Koper, M., Nitrate reduction on single-crystal platinum electrodes. *Electrochim. Acta* **2005,** *50* (21), 4318-4326.
31. Taguchi, S.; Feliu, J. M., Electrochemical reduction of nitrate on Pt (S)[n (111)×(111)] electrodes in perchloric acid solution. *Electrochim. Acta* **2007,** *52* (19), 6023-6033.
32. Dima, G.; De Vooys, A.; Koper, M., Electrocatalytic reduction of nitrate at low concentration on coinage and transition-metal electrodes in acid solutions. *J. Electroanal. Chem.* **2003,** *554*, 15-23.
33. Yang, J.; Sebastian, P.; Duca, M.; Hoogenboom, T.; Koper, M. T., pH dependence of the electroreduction of nitrate on Rh and Pt polycrystalline electrodes. *Chemical Communications* **2014,** *50* (17), 2148-2151.
34. Brylev, O.; Sarrazin, M.; Bélanger, D.; Roué, L., Rhodium deposits on pyrolytic graphite substrate: Physico-chemical properties and electrocatalytic activity towards nitrate reduction in neutral medium. *Appl. Catal. B* **2006,** *64* (3), 243-253.
35. Duca, M.; van der Klugt, B.; Koper, M., Electrocatalytic reduction of nitrite on transition and coinage metals. *Electrochim. Acta* **2012,** *68*, 32-43.
36. Badea, G. E., Electrocatalytic reduction of nitrate on copper electrode in alkaline solution. *Electrochim. Acta* **2009,** *54* (3), 996-1001.
37. Reyter, D.; Bélanger, D.; Roué, L., Study of the electroreduction of nitrate on copper in alkaline solution. *Electrochim. Acta* **2008,** *53* (20), 5977-5984.
38. Bouzek, K.; Paidar, M.; Sadilkova, A.; Bergmann, H., Electrochemical reduction of nitrate in weakly alkaline solutions. *J. Appl. Electrochem.* **2001,** *31* (11), 1185-1193.
39. Yang, H.; Xu, Z.; Fan, M.; Gupta, R.; Slimane, R. B.; Bland, A. E.; Wright, I., Progress in carbon dioxide separation and capture: A review. *Journal of environmental sciences* **2008,** *20* (1), 14-27.

40. Yamasaki, A., An overview of CO2 mitigation options for global warming—emphasizing CO2 sequestration options. *Journal of Chemical Engineering of Japan* **2003,** *36* (4), 361-375.
41. Huijgen, W. J. J.; Comans, R. N. J. *Carbon dioxide sequestration by mineral carbonation. Literature Review*; Energy research Centre of the Netherlands ECN: 2003.
42. Hori, Y.; Kikuchi, K.; Suzuki, S., Production of CO and CH4 in electrochemical reduction of CO2 at metal electrodes in aqueous hydrogencarbonate solution. *Chem. Lett.* **1985,** *14* (11), 1695-1698.
43. Noda, H.; Ikeda, S.; Oda, Y.; Imai, K.; Maeda, M.; Ito, K., Electrochemical reduction of carbon dioxide at various metal electrodes in aqueous potassium hydrogen carbonate solution. *Bull. Chem. Soc. Jpn.* **1990,** *63* (9), 2459-2462.
44. Hansen, H.; Varley, J.; Peterson, A.; Norskov, J.; Nørskov, J., Understanding Trends in the Electrocatalytic Activity of Metals and Enzymes for CO2Reduction to CO. *J. Phys. Chem. Lett.* **2013,** *4* (3), 388-392.
45. Sullivan, B. P.; Krist, K.; Guard, H., *Electrochemical and electrocatalytic reactions of carbon dioxide*. Elsevier: 2012.
46. Summers, D. P.; Leach, S.; Frese, K. W., The electrochemical reduction of aqueous carbon dioxide to methanol at molybdenum electrodes with low overpotentials. *J. Electroanal. Chem. Interfacial Electrochem.* **1986,** *205* (1-2), 219-232.
47. Hori, Y.; Takahashi, I.; Koga, O.; Hoshi, N., Selective formation of C2 compounds from electrochemical reduction of CO2 at a series of copper single crystal electrodes. *J. Phys. Chem. B* **2002,** *106* (1), 15-17.
48. Li, C. W.; Ciston, J.; Kanan, M. W., Electroreduction of carbon monoxide to liquid fuel on oxide-derived nanocrystalline copper. *Nature* **2014,** *508* (7497), 504-507.
49. Gattrell, M.; Gupta, N.; Co, A., A review of the aqueous electrochemical reduction of CO 2 to hydrocarbons at copper. *J. Electroanal. Chem.* **2006,** *594* (1), 1-19.
50. Kuhl, K. P.; Cave, E. R.; Abram, D. N.; Jaramillo, T. F., New insights into the electrochemical reduction of carbon dioxide on metallic copper surfaces. *Energy Environ. Sci.* **2012,** *5* (5), 7050-7059.
51. Schouten, K.; Kwon, Y.; Van der Ham, C.; Qin, Z.; Koper, M., A new mechanism for the selectivity to C 1 and C 2 species in the electrochemical reduction of carbon dioxide on copper electrodes. *Chem. Sci.* **2011,** *2* (10), 1902-1909.

52. Kortlever, R.; Shen, J.; Schouten, K. J. P.; Calle-Vallejo, F.; Koper, M. T., Catalysts and reaction pathways for the electrochemical reduction of carbon dioxide. *J. Phys. Chem. Lett.* **2015,** *6* (20), 4073-4082.
53. Calle‐Vallejo, F.; Koper, M., Theoretical considerations on the electroreduction of CO to C2 species on Cu (100) electrodes. *Angew. Chem. Int. Ed.* **2013,** *52* (28), 7282-7285.
54. Li, H.; Li, Y.; Koper, M. T.; Calle-Vallejo, F., Bond-making and breaking between carbon, nitrogen, and oxygen in electrocatalysis. *J. Am. Chem. Soc.* **2014,** *136* (44), 15694-15701.
55. Verdaguer-Casadevall, A.; Li, C. W.; Johansson, T. P.; Scott, S. B.; McKeown, J. T.; Kumar, M.; Stephens, I. E.; Kanan, M. W.; Chorkendorff, I., Probing the active surface sites for CO reduction on oxide-derived copper electrocatalysts. *J. Am. Chem. Soc.* **2015,** *137* (31), 9808-9811.
56. Varela, A. S.; Ju, W.; Reier, T.; Strasser, P., Tuning the Catalytic Activity and Selectivity of Cu for CO2 Electroreduction in the Presence of Halides. *ACS Catal.* **2016,** *6* (4), 2136-2144.
57. Peterson, A. A.; Abild-Pedersen, F.; Studt, F.; Rossmeisl, J.; Nørskov, J. K., How copper catalyzes the electroreduction of carbon dioxide into hydrocarbon fuels. *Energy Environ. Sci.* **2010,** *3* (9), 1311-1315.
58. Montoya, J. H.; Shi, C.; Chan, K.; Nørskov, J. K., Theoretical Insights into a CO Dimerization Mechanism in CO2 Electroreduction. *J. Phys. Chem. Lett.* **2015,** *6* (11), 2032-2037.
59. Schouten, K. J. P.; Qin, Z.; Gallent, E. P.; Koper, M. T. M., Two Pathways for the Formation of Ethylene in CO Reduction on Single-Crystal Copper Electrodes. *J. Am. Chem. Soc.* **2012,** *134* (24), 9864-9867.
60. Hori, Y.; Wakebe, H.; Tsukamoto, T.; Koga, O., Electrocatalytic process of CO selectivity in electrochemical reduction of CO2 at metal electrodes in aqueous media. *Electrochim. Acta* **1994,** *39* (11–12), 1833-1839.
61. Hori, Y.; Takahashi, R.; Yoshinami, Y.; Murata, A., Electrochemical reduction of CO at a copper electrode. *J. Phys. Chem. B* **1997,** *101* (36), 7075-7081.
62. Hori, Y.; Murata, A.; Takahashi, R.; Suzuki, S., Electroreduction of CO to CH/sub 4/and C/sub 2/H/sub 4/at a copper electrode in aqueous solutions at ambient temperature and pressure. *J. Am. Chem. Soc.;(United States)* **1987,** *109* (16).
63. Schouten, K. J. P.; Gallent, E. P.; Koper, M. T., The influence of pH on the reduction of CO and CO2 to hydrocarbons on copper electrodes. *J. Electroanal. Chem.* **2014,** *716*, 53-57.

64. Schouten, K. J. P.; Pérez Gallent, E.; Koper, M. T., Structure sensitivity of the electrochemical reduction of carbon monoxide on copper single crystals. *ACS Catal.* **2013,** *3* (6), 1292-1295.
65. Murata, A.; Hori, Y., Product selectivity affected by cationic species in electrochemical reduction of CO2 and CO at a Cu electrode. *Bull. Chem. Soc. Jpn.* **1991,** *64* (1), 123-127.
66. Kas, R.; Kortlever, R.; Milbrat, A.; Koper, M. T.; Mul, G.; Baltrusaitis, J., Electrochemical CO 2 reduction on Cu 2 O-derived copper nanoparticles: controlling the catalytic selectivity of hydrocarbons. *Phys. Chem. Chem. Phys.* **2014,** *16* (24), 12194-12201.
67. Christophe, J.; Doneux, T.; Buess Herman, C., Electroreduction of Carbon Dioxide on Copper-Based Electrodes: Activity of Copper Single Crystals and Copper–Gold Alloys. *Electrocatalysis* **2012,** *3* (2), 139-146.
68. Angamuthu, R.; Byers, P.; Lutz, M.; Spek, A. L.; Bouwman, E., Electrocatalytic CO2 conversion to oxalate by a copper complex. *Science* **2010,** *327* (5963), 313-315.
69. Tundo, P.; Selva, M., The chemistry of dimethyl carbonate. *Acc. Chem. Res.* **2002,** *35* (9), 706-716.
70. Sakakura, T.; Choi, J.-C.; Yasuda, H., Transformation of carbon dioxide. *Chem. Rev* **2007,** *107* (6), 2365-2387.
71. Evison, D.; Hinsley, D.; Rice, P., Chemical weapons. *BMJ : British Medical Journal* **2002,** *324* (7333), 332-335.
72. North, M.; Pasquale, R., Mechanism of cyclic carbonate synthesis from epoxides and CO2. *Angew. Chem.* **2009,** *121* (16), 2990-2992.
73. Korosteleva, I.; Markova, N.; Kolesnichenko, N.; Ezhova, N.; Khadzhiev, S.; Trukhmanova, N., Catalytic synthesis of propylene carbonate from propylene oxide and carbon dioxide in the presence of rhodium complexes modified with organophosphorus ligands and chitosan. *Petroleum Chemistry* **2013,** *53* (6), 412-417.
74. Foltran, S.; Mereau, R.; Tassaing, T., Theoretical study on the chemical fixation of carbon dioxide with propylene oxide catalyzed by ammonium and guanidinium salts. *Catal. Sci. Technol.* **2014,** *4* (6), 1585-1597.
75. Baiker, A., Utilization of carbon dioxide in heterogeneous catalytic synthesis². **2000**.
76. Darensbourg, D. J.; Holtcamp, M. W., Catalysts for the reactions of epoxides and carbon dioxide. *Coordination Chemistry Reviews* **1996,** *153*, 155-174.
77. Shaikh, A.-A. G.; Sivaram, S., Organic carbonates. *Chem. Rev.* **1996,** *96* (3), 951-976.

78. Yang, H.; Gu, Y.; Deng, Y.; Shi, F., Electrochemical activation of carbon dioxide in ionic liquid: synthesis of cyclic carbonates at mild reaction conditions. *Chemical Communications* **2002,** (3), 274-275.
79. Buckley, B. R.; Patel, A. P.; Wijayantha, K. U., Electrosynthesis of cyclic carbonates from epoxides and atmospheric pressure carbon dioxide. *Chemical Communications* **2011,** *47* (43), 11888-11890.
80. Wu, L.; Yang, H.; Wang, H.; Lu, J., Electrosynthesis of cyclic carbonates from CO 2 and epoxides on a reusable copper nanoparticle cathode. *RSC Adv.* **2015,** *5* (30), 23189-23192.
81. Wang, H.; Wu, L.-X.; Lan, Y.-C.; Zhao, J.-Q.; Lu, J.-X., Electrosynthesis of cyclic carbonates from CO2 and diols in ionic liquids under mild conditions. *Int. J. Electrochem. Sci* **2011,** *6*, 4218-4227.
82. Kihara, N.; Nakawaki, Y.; Endo, T., Preparation of 1, 3-oxathiolane-2-thiones by the reaction of oxirane and carbon disulfide. *The Journal of Organic Chemistry* **1995,** *60* (2), 473-475.
83. Calo, V.; Nacci, A.; Monopoli, A.; Fanizzi, A., Cyclic carbonate formation from carbon dioxide and oxiranes in tetrabutylammonium halides as solvents and catalysts. *Organic letters* **2002,** *4* (15), 2561-2563.
84. Xiao, Y.; Chen, B.-L.; Yang, H.-P.; Wang, H.; Lu, J.-X., Electrosynthesis of enantiomerically pure cyclic carbonates from CO 2 and chiral epoxides. *Electrochem. Commun.* **2014,** *43*, 71-74.
85. Schmitz, C., The Rise of Big Business in the World Copper Industry 1870-1930. *The Economic History Review* **1986,** *39* (3), 392-410.
86. Hori, Y.; Kikuchi, K.; Murata, A.; Suzuki, S., Production of methane and ethylene in electrochemical reduction of carbon dioxide at copper electrode in aqueous hydrogencarbonate solution. *Chem. Lett.* **1986,** *15* (6), 897-898.
87. Vitousek, P. M.; Howarth, R. W., Nitrogen Limitation on Land and in the Sea: How Can It Occur? *Biogeochemistry* **1991,** *13* (2), 87-115.
88. Galloway, J. N.; Townsend, A. R.; Erisman, J. W.; Bekunda, M.; Cai, Z.; Freney, J. R.; Martinelli, L. A.; Seitzinger, S. P.; Sutton, M. A., Transformation of the Nitrogen Cycle: Recent Trends, Questions, and Potential Solutions. *Science* **2008,** *320* (5878), 889-892.
89. Duca, M.; Kavvadia, V.; Rodriguez, P.; Lai, S. C. S.; Hoogenboom, T.; Koper, M. T. M., New insights into the mechanism of nitrite reduction on a platinum electrode. *J. Electroanal. Chem.* **2010,** *649* (1–2), 59-68.
90. Bae, S.-E.; Gewirth, A. A., Differential reactivity of Cu (111) and Cu (100) during nitrate reduction in acid electrolyte. *Faraday Discuss.* **2009,** *140*, 113-123.

91. Schouten, K. J. P.; Gallent, E. P.; Koper, M. T., The electrochemical characterization of copper single-crystal electrodes in alkaline media. *J. Electroanal. Chem.* **2013,** *699*, 6-9.
92. Wonders, A. H.; Housmans, T. H. M.; Rosca, V.; Koper, M. T. M., On-line mass spectrometry system for measurements at single-crystal electrodes in hanging meniscus configuration. *J. Appl. Electrochem.* **2006,** *36* (11), 1215-1221.
93. Yang, J.; Kwon, Y.; Duca, M.; Koper, M. T., Combining Voltammetry and Ion Chromatography: Application to the Selective Reduction of Nitrate on Pt and PtSn Electrodes. *Analytical chemistry* **2013,** *85* (16), 7645-7649.
94. Figueiredo, M. C.; Souza-Garcia, J.; Climent, V.; Feliu, J. M., Nitrate reduction on Pt (111) surfaces modified by Bi adatoms. *Electrochem. Commun.* **2009,** *11* (9), 1760-1763.
95. Bae, S.-E.; Stewart, K. L.; Gewirth, A. A., Nitrate adsorption and reduction on Cu (100) in acidic solution. *J. Am. Chem. Soc.* **2007,** *129* (33), 10171-10180.
96. Petrii, O. A.; Safonova, T. Y., Electroreduction of nitrate and nitrite anions on platinum metals: a model process for elucidating the nature of the passivation by hydrogen adsorption. *J. Electroanal. Chem.* **1992,** *331* (1), 897-912.
97. Horanyi, G.; Rizmayer, E., Role of adsorption phenomena in the electrocatalytic reduction of nitric acid at a platinized platinum electrode. *J. Electroanal. Chem. Interfacial Electrochem.* **1982,** *140* (2), 347-366.
98. Koper, M. T., Non-linear phenomena in electrochemical systems. *Journal of the Chemical Society, Faraday Transactions* **1998,** *94* (10), 1369-1378.
99. Rosca, V.; Beltramo, G. L.; Koper, M. T. M., Hydroxylamine electrochemistry at polycrystalline platinum in acidic media: a voltammetric, DEMS and FTIR study. *J. Electroanal. Chem.* **2004,** *566* (1), 53-62.
100. Rodes, A.; Gomez, R.; Orts, J.; Feliu, J.; Perez, J.; Aldaz, A., In situ FTIR spectroscopy characterization of the NO adlayers formed at platinum single crystal electrodes in contact with acidic solutions of nitrite. *Langmuir* **1995,** *11* (9), 3549-3553.
101. Hughes, M.; Nicklin, H.; Shrimanker, K., Autoxidation of hydroxylamine in alkaline solutions. Part II. Kinetics. The acid dissociation constant of hydroxylamine. *Journal of the Chemical Society A: Inorganic, Physical, Theoretical* **1971**, 3485-3487.

102. Dumas, P.; Suhren, M.; Chabal, Y.; Hirschmugl, C.; Williams, G., Adsorption and reactivity of NO on Cu (111): a synchrotron infrared reflection absorption spectroscopic study. *Surf. Sci.* **1997,** *371* (2), 200-212.
103. Kim, C.; Yi, C.-W.; Goodman, D., Adsorption and reaction of NO on Cu (100): an infrared reflection absorption spectroscopic study at 25 K. *J. Phys. Chem. B* **2002,** *106* (28), 7065-7068.
104. Santos, E.; Pötting, K.; Lundin, A.; Quaino, P.; Schmickler, W., Hydrogen Evolution on Single‐Crystal Copper and Silver: A Theoretical Study. *ChemPhysChem* **2010,** *11* (7), 1491-1495.
105. Gattrell, M.; Gupta, N.; Co, A., A review of the aqueous electrochemical reduction of CO2 to hydrocarbons at copper. *Journal of Electroanalytical Chemistry* **2006,** *594* (1), 1-19.
106. Hori, Y.; Murata, A.; Takahashi, R., Formation of hydrocarbons in the electrochemical reduction of carbon dioxide at a copper electrode in aqueous solution. *Journal of the Chemical Society, Faraday Transactions 1: Physical Chemistry in Condensed Phases* **1989,** *85* (8), 2309-2326.
107. Calle-Vallejo, F.; Koper, M. T. M., Theoretical Considerations on the Electroreduction of CO to C2 Species on Cu(100) Electrodes. *Angewandte Chemie International Edition* **2013,** *52* (28), 7282-7285.
108. Schouten, K. J. P.; Calle-Vallejo, F.; Koper, M. T. M., A Step Closer to the Electrochemical Production of Liquid Fuels. *Angewandte Chemie International Edition* **2014,** *53* (41), 10858-10860.
109. Schouten, K. J. P.; Kwon, Y.; van der Ham, C. J. M.; Qin, Z.; Koper, M. T. M., A new mechanism for the selectivity to C1 and C2 species in the electrochemical reduction of carbon dioxide on copper electrodes. *Chemical Science* **2011,** *2* (10), 1902.
110. P. Schouten, K. J.; Gallent, E. P.; Koper, M. T. M., The electrochemical characterization of copper single-crystal electrodes in alkaline media. *Journal of Electroanalytical Chemistry* **2013,** *699* (0), 6-9.
111. Kwon, Y.; Koper, M. T. M., Combining Voltammetry with HPLC: Application to Electro-Oxidation of Glycerol. *Analytical Chemistry* **2010,** *82* (13), 5420-5424.
112. Kresse, G.; Furthmüller, J., Efficient iterative schemes for ab initio total-energy calculations using a plane-wave basis set. *Physical Review B* **1996,** *54* (16), 11169-11186.
113. Perdew, J. P.; Burke, K.; Ernzerhof, M., Generalized Gradient Approximation Made Simple. *Physical Review Letters* **1996,** *77* (18), 3865-3868.

114. Kresse, G.; Joubert, D., From ultrasoft pseudopotentials to the projector augmented-wave method. *Physical Review B* **1999,** *59* (3), 1758-1775.
115. Monkhorst, H. J.; Pack, J. D., Special points for Brillouin-zone integrations. *Physical Review B* **1976,** *13* (12), 5188-5192.
116. Methfessel, M.; Paxton, A. T., High-precision sampling for Brillouin-zone integration in metals. *Physical Review B* **1989,** *40* (6), 3616-3621.
117. Lide, D. R., *CRC Handbook of Chemistry and Physics. ed. CD-ROM version*. 90th ed.; CRC Press/Taylor and Francis: Boca Raton, FL, 2010.
118. Calle-Vallejo, F.; Koper, M. T. M., First-principles computational electrochemistry: Achievements and challenges. *Electrochimica Acta* **2012,** *84*, 3-11.
119. Norskov, J. K.; Rossmeisl, J.; Logadottir, A.; Lindqvist, L.; Kitchin, J. R.; Bligaard, T.; Jonsson, H., Origin of the overpotential for oxygen reduction at a fuel-cell cathode. *Journal of Physical Chemistry B* **2004,** *108* (46), 17886-17892.
120. Peterson, A. A.; Abild-Pedersen, F.; Studt, F.; Rossmeisl, J.; Norskov, J. K., How copper catalyzes the electroreduction of carbon dioxide into hydrocarbon fuels. *Energy & Environmental Science* **2010,** *3* (9), 1311-1315.
121. Nørskov, J. K.; Rossmeisl, J.; Logadottir, A.; Lindqvist, L.; Kitchin, J. R.; Bligaard, T.; Jónsson, H., Origin of the Overpotential for Oxygen Reduction at a Fuel-Cell Cathode. *J. Phys. Chem. B* **2004,** *108* (46), 17886-17892.
122. Li, H.; Li, Y.; Koper, M. T. M.; Calle-Vallejo, F., Bond-Making and Breaking between Carbon, Nitrogen, and Oxygen in Electrocatalysis. *Journal of the American Chemical Society* **2014,** *136* (44), 15694-15701.
123. Calle-Vallejo, F.; Martínez, J. I.; García-Lastra, J. M.; Sautet, P.; Loffreda, D., Fast Prediction of Adsorption Properties for Platinum Nanocatalysts with Generalized Coordination Numbers. *Angewandte Chemie International Edition* **2014,** *53* (32), 8316-8319.
124. Calle-Vallejo, F.; Loffreda, D.; KoperMarc, T. M.; Sautet, P., Introducing structural sensitivity into adsorption–energy scaling relations by means of coordination numbers. *Nat Chem* **2015,** *7* (5), 403-410.
125. Calle-Vallejo, F.; Huang, M.; Henry, J. B.; Koper, M. T. M.; Bandarenka, A. S., Theoretical design and experimental implementation of Ag/Au electrodes for the electrochemical reduction of nitrate. *Physical Chemistry Chemical Physics* **2013,** *15* (9), 3196-3202.
126. Zhang, Y.-J.; Sethuraman, V.; Michalsky, R.; Peterson, A. A., Competition between CO2 Reduction and H2 Evolution on Transition-Metal Electrocatalysts. *ACS Catalysis* **2014,** *4* (10), 3742-3748.

127. Ledezma-Yanez, I.; Gallent, E. P.; Koper, M. T.; Calle-Vallejo, F., Structure-sensitive electroreduction of acetaldehyde to ethanol on copper and its mechanistic implications for CO and CO 2 reduction. *Catal. Today* **2016,** *262*, 90-94.
128. Garcia, G.; Rodriguez, P.; Rosca, V.; Koper, M., Fourier transform infrared spectroscopy study of CO electro-oxidation on Pt (111) in alkaline media. *Langmuir* **2009,** *25* (23), 13661-13666.
129. Hori, Y.; Koga, O.; Watanabe, Y.; Matsuo, T., FTIR measurements of charge displacement adsorption of CO on poly-and single crystal (100) of Cu electrodes. *Electrochim. Acta* **1998,** *44* (8), 1389-1395.
130. Ryberg, R., Carbon monoxide adsorbed on Cu(100) Studied by infrared spectroscopy. *Surf. Sci.* **1982,** *114* (2), 627-641.
131. Gajdoš, M.; Hafner, J., CO adsorption on Cu(1 1 1) and Cu(0 0 1) surfaces: Improving site preference in DFT calculations. *Surf. Sci.* **2005,** *590* (2–3), 117-126.
132. Chang, S. C.; Weaver, M. J., In situ infrared spectroscopy of carbon monoxide adsorbed at ordered platinum (100)-aqueous interfaces: double-layer effects upon the adsorbate binding geometry. *J. Phys. Chem.* **1990,** *94* (12), 5095-5102.
133. Arán-Ais, R. M.; Figueiredo, M. C.; Vidal-Iglesias, F. J.; Climent, V.; Herrero, E.; Feliu, J. M., On the behavior of the Pt (100) and vicinal surfaces in alkaline media. *Electrochim. Acta* **2011,** *58*, 184-192.
134. Shaw, S. K.; Berná, A.; Feliu, J. M.; Nichols, R. J.; Jacob, T.; Schiffrin, D. J., Role of axially coordinated surface sites for electrochemically controlled carbon monoxide adsorption on single crystal copper electrodes. *Phys. Chem. Chem. Phys.* **2011,** *13* (12), 5242-5251.
135. Koper, M. T.; van Santen, R. A., Electric field effects on CO and NO adsorption at the Pt (111) surface. *J. Electroanal. Chem.* **1999,** *476* (1), 64-70.
136. Socrates, G., *Infrared and Raman characteristic group frequencies: tables and charts*. John Wiley & Sons: 2004.
137. Severson, M. W.; Stuhlmann, C.; Villegas, I.; Weaver, M. J., Dipole–dipole coupling effects upon infrared spectroscopy of compressed electrochemical adlayers: Application to the Pt (111)/CO system. *J. Chem. Phys.* **1995,** *103* (22), 9832-9843.
138. Calle-Vallejo, F.; Ignacio Martinez, J.; Rossmeisl, J., Density functional studies of functionalized graphitic materials with late transition metals for oxygen reduction reactions. *Phys. Chem. Chem. Phys.* **2011,** *13* (34), 15639-15643.

139. Maier, G.; Rohr, C., Ethynediol: Photochemical Generation and Matrix‐spectroscopic Identification. *Liebigs Ann.* **1996,** *1996* (3), 307-309.
140. Calle-Vallejo, F.; Martínez, J. I.; García-Lastra, J. M.; Abad, E.; Koper, M. T. M., Oxygen reduction and evolution at single-metal active sites: Comparison between functionalized graphitic materials and protoporphyrins. *Surf. Sci.* **2013,** *607*, 47-53.
141. Nie, X.; Esopi, M. R.; Janik, M. J.; Asthagiri, A., Selectivity of CO2 reduction on copper electrodes: the role of the kinetics of elementary steps. *Angew. Chem. Int. Ed.* **2013,** *52* (9), 2459-2462.
142. Hori, Y., Electrochemical CO2 reduction on metal electrodes. In *Modern aspects of electrochemistry*, Springer: 2008; pp 89-189.
143. Roberts, F. S.; Kuhl, K. P.; Nilsson, A., High selectivity for ethylene from carbon dioxide reduction over copper nanocube electrocatalysts. *Angew. Chem. Int. Ed.* **2015,** *54* (17), 5179-5182.
144. Hori, Y.; Takahashi, I.; Koga, O.; Hoshi, N., Electrochemical reduction of carbon dioxide at various series of copper single crystal electrodes. *J. Mol. Catal. A: Chem.* **2003,** *199* (1), 39-47.
145. Lee, S.; Kim, D.; Lee, J., Electrocatalytic Production of C3‐C4 Compounds by Conversion of CO2 on a Chloride‐Induced Bi‐Phasic Cu2O‐Cu Catalyst. *Angew. Chem.* **2015,** *127* (49), 14914-14918.
146. Kyriacou, G.; Anagnostopoulos, A., Influence CO 2 partial pressure and the supporting electrolyte cation on the product distribution in CO 2 electroreduction. *J. Appl. Electrochem.* **1993,** *23* (5), 483-486.
147. Singh, M. R.; Kwon, Y.; Lum, Y.; Ager III, J. W.; Bell, A. T., Hydrolysis of Electrolyte Cations Enhances the Electrochemical Reduction of CO2 over Ag and Cu. *J. Am. Chem. Soc.* **2016,** *138* (39), 13006-13012.
148. Wuttig, A.; Surendranath, Y., Impurity ion complexation enhances carbon dioxide reduction catalysis. *ACS Catal.* **2015,** *5* (7), 4479-4484.
149. Birdja, Y. Y.; Koper, M. T. M., The Importance of Cannizzaro-Type Reactions during Electrocatalytic Reduction of Carbon Dioxide. *J. Am. Chem. Soc.* **2017,** *139* (5), 2030-2034.
150. Pérez‐Gallent, E.; Figueiredo, M. C.; Calle‐Vallejo, F.; Koper, M., Spectroscopic Observation of a Hydrogenated CO Dimer Intermediate During CO Reduction on Cu (100) Electrodes. *Angew. Chem.* **2017,** *129* (13), 3675-3678.
151. Cook, R. L.; MacDuff, R. C.; Sammells, A. F., Evidence for formaldehyde, formic acid, and acetaldehyde as possible intermediates during electrochemical carbon dioxide reduction at copper. *J. Electrochem. Soc.* **1989,** *136* (7), 1982-1984.

152. DeWulf, D. W.; Jin, T.; Bard, A. J., Electrochemical and surface studies of carbon dioxide reduction to methane and ethylene at copper electrodes in aqueous solutions. *J. Electrochem. Soc.* **1989,** *136* (6), 1686-1691.
153. Akhade, S. A.; McCrum, I. T.; Janik, M. J., The impact of specifically adsorbed ions on the copper-Catalyzed electroreduction of CO2. *J. Electrochem. Soc.* **2016,** *163* (6), F477-F484.
154. Sandberg, R. B.; Montoya, J. H.; Chan, K.; Nørskov, J. K., CO-CO coupling on Cu facets: Coverage, strain and field effects. *Surf. Sci.* **2016,** *654*, 56-62.
155. Chen, L. D.; Urushihara, M.; Chan, K.; Nørskov, J. K., Electric Field Effects in Electrochemical CO2 Reduction. *ACS Catal.* **2016,** *6* (10), 7133-7139.
156. Kim, Y.-G.; Javier, A.; Baricuatro, J. H.; Soriaga, M. P., Regulating the product distribution of CO reduction by the atomic-level structural modification of the Cu electrode surface. *Electrocatalysis* **2016,** *7* (5), 391-399.
157. Gao, D.; Zegkinoglou, I.; Divins, N. J.; Scholten, F.; Sinev, I.; Grosse, P.; Roldan Cuenya, B., Plasma-Activated Copper Nanocube Catalysts for Efficient Carbon Dioxide Electroreduction to Hydrocarbons and Alcohols. *ACS nano* **2017,** *11* (5), 4825-4831.
158. Bertheussen, E.; Verdaguer‐Casadevall, A.; Ravasio, D.; Montoya, J. H.; Trimarco, D. B.; Roy, C.; Meier, S.; Wendland, J.; Nørskov, J. K.; Stephens, I. E., Acetaldehyde as an Intermediate in the Electroreduction of Carbon Monoxide to Ethanol on Oxide‐Derived Copper. *Angew. Chem. Int. Ed.* **2016,** *55* (4), 1450-1454.
159. Rochelle, C.; Czernichowski-Lauriol, I.; Milodowski, A., The impact of chemical reactions on CO2 storage in geological formations: a brief review. *Geological Society, London, Special Publications* **2004,** *233* (1), 87-106.
160. Jasinski, R., Bibliography on the uses of propylene carbonate in high energy, density batteries. *J. Electroanal. Chem. Interfacial Electrochem.* **1967,** *15*, 89-91.
161. Bhanage, B. M.; Fujita, S.-i.; Ikushima, Y.; Arai, M., Synthesis of dimethyl carbonate and glycols from carbon dioxide, epoxides, and methanol using heterogeneous basic metal oxide catalysts with high activity and selectivity. *Applied Catalysis A: General* **2001,** *219* (1), 259-266.
162. Zhang, L.; Niu, D.; Zhang, K.; Zhang, G.; Luo, Y.; Lu, J., Electrochemical activation of CO 2 in ionic liquid (BMIMBF 4): synthesis of

organic carbonates under mild conditions. *Green Chemistry* **2008,** *10* (2), 202-206.
163. Lu, X.-B.; Wang, H.; He, R., Aluminum phthalocyanine complex covalently bonded to MCM-41 silica as heterogeneous catalyst for the synthesis of cyclic carbonates. *J. Mol. Catal. A: Chem.* **2002,** *186* (1), 33-42.
164. Figueiredo, M. C.; Ledezma-Yanez, I.; Koper, M. T., In situ spectroscopic study of CO2 electroreduction at copper electrodes in acetonitrile. *ACS Catal.* **2016,** *6* (4), 2382-2392.
165. Ledezma-Yanez, I.; Koper, M. T. M., Influence of water on the hydrogen evolution reaction on a gold electrode in acetonitrile solution. *J. Electroanal. Chem.* **2017,** *793* (Supplement C), 18-24.
166. Christensen, P.; Hamnett, A.; Muir, A.; Freeman, N., CO2 reduction at platinum, gold and glassy carbon electrodes in acetonitrile: An in-situ FTIR study. *J. Electroanal. Chem. Interfacial Electrochem.* **1990,** *288* (1-2), 197-215.
167. Foley, J. K.; Korzeniewski, C.; Pons, S., Anodic and cathodic reactions in acetonitrile/tetra-n-butylammonium tetrafluoroborate: an electrochemical and infrared spectroelectrochemical study. *Canadian journal of chemistry* **1988,** *66* (1), 201-206.
168. Hori, Y.; Murata, A.; Yoshinami, Y., Adsorption of CO, intermediately formed in electrochemical reduction of CO2, at a copper electrode. *Journal of the Chemical Society, Faraday Transactions* **1991,** *87* (1), 125-128.
169. Wuttig, A.; Liu, C.; Peng, Q.; Yaguchi, M.; Hendon, C. H.; Motobayashi, K.; Ye, S.; Osawa, M.; Surendranath, Y., Tracking a common surface-bound intermediate during CO2-to-fuels catalysis. *ACS central science* **2016,** *2* (8), 522-528.
170. Wang, W.; Li, C.; Yan, L.; Wang, Y.; Jiang, M.; Ding, Y., Ionic liquid/Zn-PPh3 integrated porous organic polymers featuring multifunctional sites: Highly active heterogeneous catalyst for cooperative conversion of CO2 to cyclic carbonates. *ACS Catal.* **2016,** *6* (9), 6091-6100.
171. Niu, K.; Xu, Y.; Wang, H.; Ye, R.; Xin, H. L.; Lin, F.; Tian, C.; Lum, Y.; Bustillo, K. C.; Doeff, M. M., A spongy nickel-organic CO2 reduction photocatalyst for nearly 100% selective CO production. *Science Advances* **2017,** *3* (7), e1700921.
172. Mills, J.; McCrum, I.; Janik, M., Alkali cation specific adsorption onto fcc (111) transition metal electrodes. *Phys. Chem. Chem. Phys.* **2014,** *16* (27), 13699-13707.
173. Jović, V. D.; Jović, B. M., EIS and differential capacitance measurements onto single crystal faces in different solutions: Part II: Cu(111) and Cu(100) in 0.1 M NaOH. *J. Electroanal. Chem.* **2003,** *541*, 13-21.

174. Marcus, Y., Thermodynamics of solvation of ions. Part 5.—Gibbs free energy of hydration at 298.15 K. *Journal of the Chemical Society, Faraday Transactions* **1991,** *87* (18), 2995-2999.
175. Ramki, C.; Vizhi, R. E., Growth, optical, electrical and mechanical properties of sodium hydrogen oxalate hydrate (NaHC 2 O 4· H 2 O) single crystal for NLO applications. *Mater. Chem. Phys.* **2017,** *197*, 70-78.

Appendix I

Supporting information to chapter 2

I.1 Results

The reduction of nitrate (NO_3^-) in a 0.1 M NaOH solution prepared in D_2O was also studied by FTIR on both copper surfaces in order to confirm the absence of the bands corresponding to NO. Figure AI.1 shows potential dependent absorbance spectra of Cu(100) (left panel) and Cu(111) (right panel) in 0.1 M NaOH solution in the presence of 10 mM $NaNO_3$. The reference spectrum is taken at +0.35 V and additional spectra are provided for +0.30, +0.25, +0.20, +0.15, +0.10, +0.05, +0.00, -0.05, -0.10, -0.15, -0.20, -0.25, -0.30, -0.35 V (all reported potentials are in the RHE scale). In agreement with the onset potentials for nitrate reduction observed in the CVs (fig. 2.1) ,IC (fig. 2.4) and FTIR (fig. 2.6), the absorbance spectra show that the onset potential for the reduction of nitrate is +0.15 V on Cu (111) and +0.1 V on Cu (100), as observed by a negative band at 1370 cm^{-1} associated with the consumption of nitrate. However, the simultaneous formation of nitrite that was observed by the positive band at 1231 cm^{-1} when the experiments were carried out in H_2O (fig. 2.6) is not observable in the experiment carried out in D_2O because the band corresponding with nitrite (NO_2^-) is masked by the D-O stretching band. There is no band at 1690 cm^{-1} that would correspond to NO, confirming the absence of formation of NO, in agreement with the results obtained with Online Mass Spectrometry (fig. 2.5).

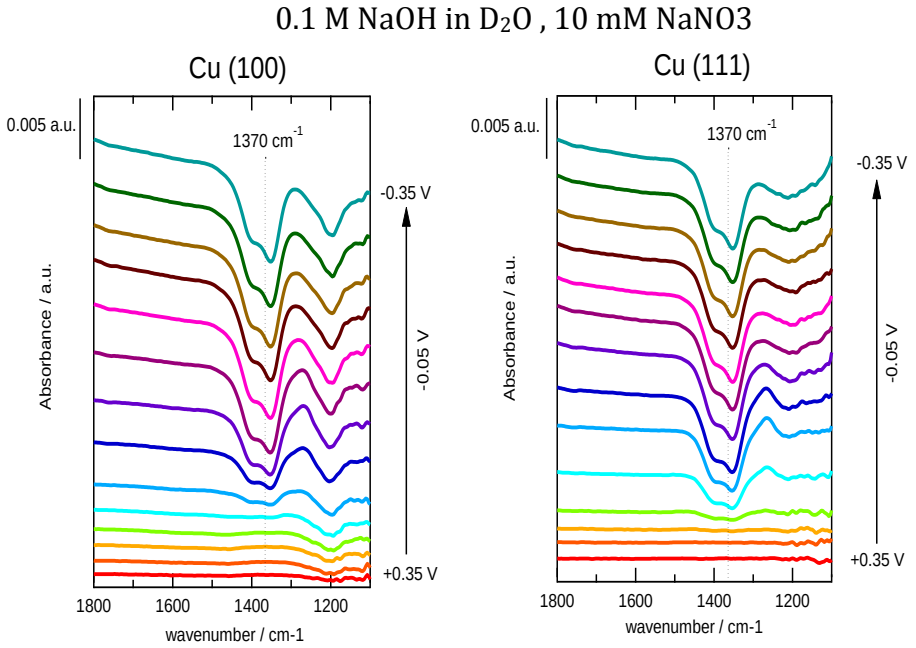

Figure AI.1: Potential dependent absorbance spectra for the reduction of 10 mM $NaNO_3$ on Cu (100) (left panel) and on Cu (111) (right panel) electrode in 0.1 M NaOH solution in D_2O. Reference spectrum recorded at 0.35 V vs. RHE. Potential step is 0.05V.

Appendix II

Supporting information to chapter 3

II.1 Voltammetric characterization of copper single-crystals electrodes

Figure AII.1 shows the characteristic features of the copper single-crystal surfaces, between -0.25 and 0.35 V_{RHE}, in agreement with those previously reported by Schouten et al [91].

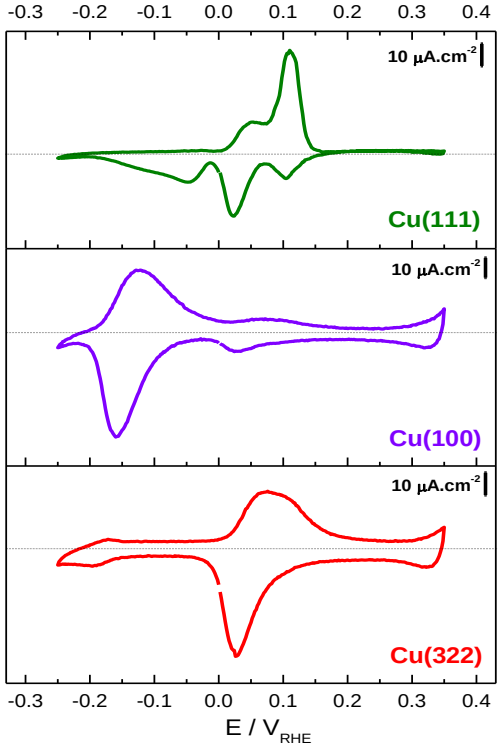

Figure AII.1: Cyclic voltammetries for Cu(111), Cu(100) and Cu(322) electrodes in 0.1 M NaOH; scan rate: 50 mV s^{-1}, Ar-atmosphere.

Figure AII.2 shows the linear sweep voltammetries for acetaldehyde reduction on three copper single-crystal surfaces, between 0.0 and -1.5 V_{RHE}, at pH 1 and 3.

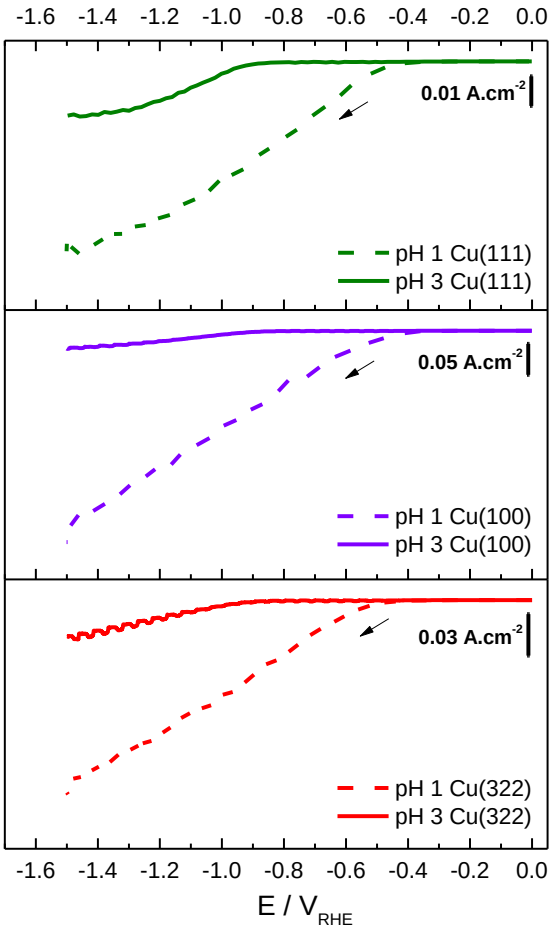

Figure AII.2: Linear sweep voltammetries for acetaldehyde reduction on Cu(111), Cu(100) and Cu(322) electrodes. The solutions used were: 0.1 M $HClO_4$ + 0.1 M acetaldehyde (pH 1), and 0.001 M $HClO_4$ + 0.099 M $KClO_4$ + 0.1 M acetaldehyde (pH 3). Scan rate: 1 mV s^{-1}, Ar-atmosphere.

II.2 DFT simulations in a high H-coverage regime

Figures AII.3 and AII.4 contain the most stable adsorption configurations of CH_3CH_2O* and CH_3*CHOH in the presence of coadsorbed hydrogen on the three crystals under study.

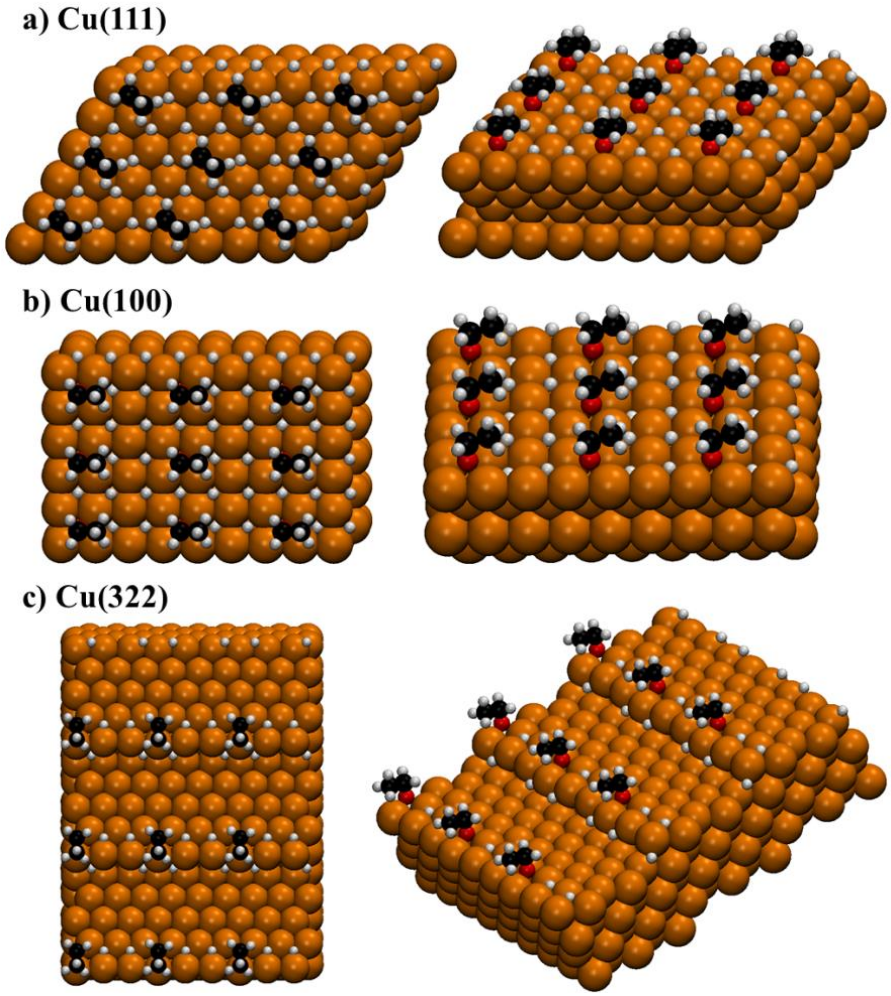

Figure AII.3: Coadsorption of *H and CH_3CH_2O* on a) Cu(111), b) Cu(100), c) Cu(322). Left: top views, right: side views.

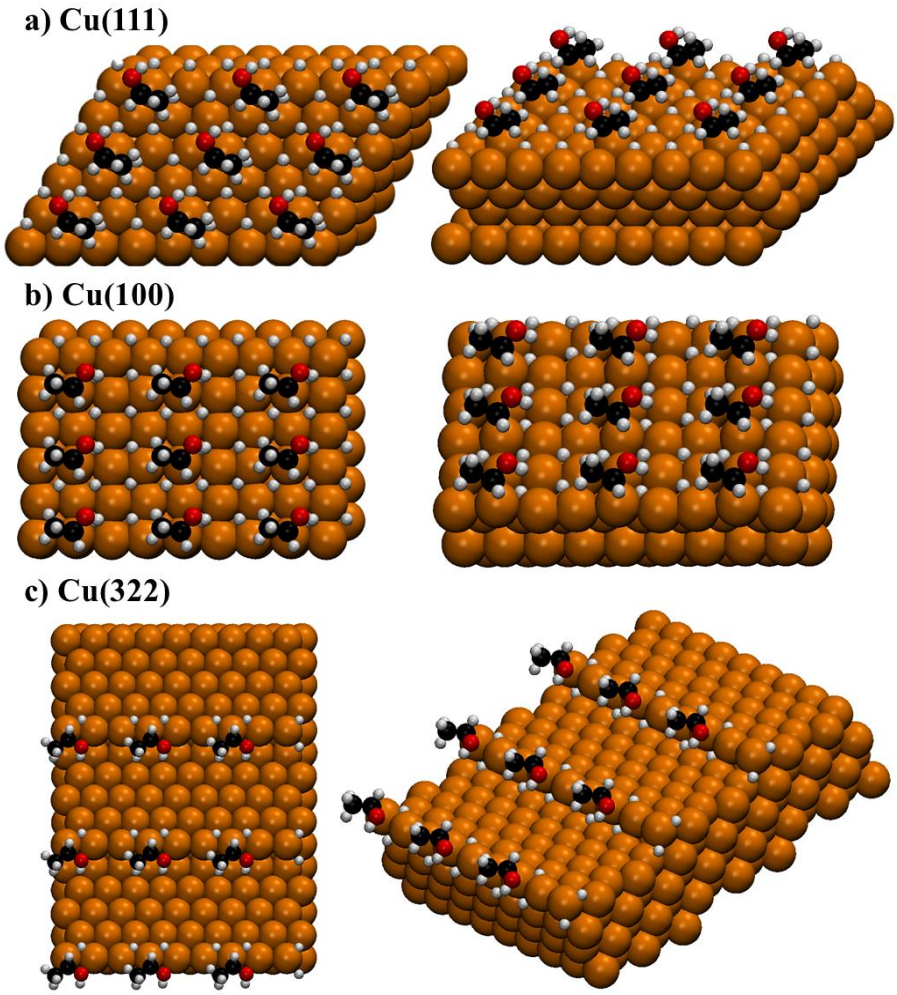

Figure AII.4: Coadsorption of *H and CH_3*CHOH on a) Cu(111), b) Cu(100), c) Cu(322). Left: top views, right: side views.

Appendix III

Supporting information to chapter 4

III.1 Results and discussion

Figure AIII.1 shows the potential-dependent absorbance spectra of Cu(111) in 0.1 M LiOH solutions in CO atmosphere. The reference spectrum is taken at +0.1 V and additional spectra are provided for +0.05, 0.00, -0.05, -0.10, -0.15 and -0.2 V (all reported potentials are on the RHE scale). The spectra show two bands at 1632 and 1407 cm^{-1} . The band at 1632 cm^{-1} corresponds to the OH bending mode of H_2O. This band causes fluctuations in the baseline of the spectra. The band at 1407 cm^{-1} is assigned to formaldehyde according to the transmission spectra obtained for this species in solution (See Figure AIII.2 e). Formaldehyde has been suggested to be an intermediate of the reduction of CO to CH_4 on Cu(211) [57]. During the reduction of CO on Cu(111), there is no band around 1680 cm^{-1} that would correspond to adsorbed CO [131]. The band at 1191 cm^{-1} that is assigned to the C-OH stretching on Cu(100) for the hydrogenated dimer is absent in the spectra obtained on Cu(111), confirming the favorability of square sites for the formation of the hydrogenated dimer as an early intermediate of CO reduction. The transmission spectra of other C1 and C2 species such as acetate, formate, acetaldehyde, formaldehyde and methanol were also recorded (Figure AIII.2). The lack of a match of the bands obtained during CO reduction with the bands observed in the transmission spectra of this C1 and C2 species, rules out the possibility of having these species as intermediates in CO reduction on Cu(100) electrodes.

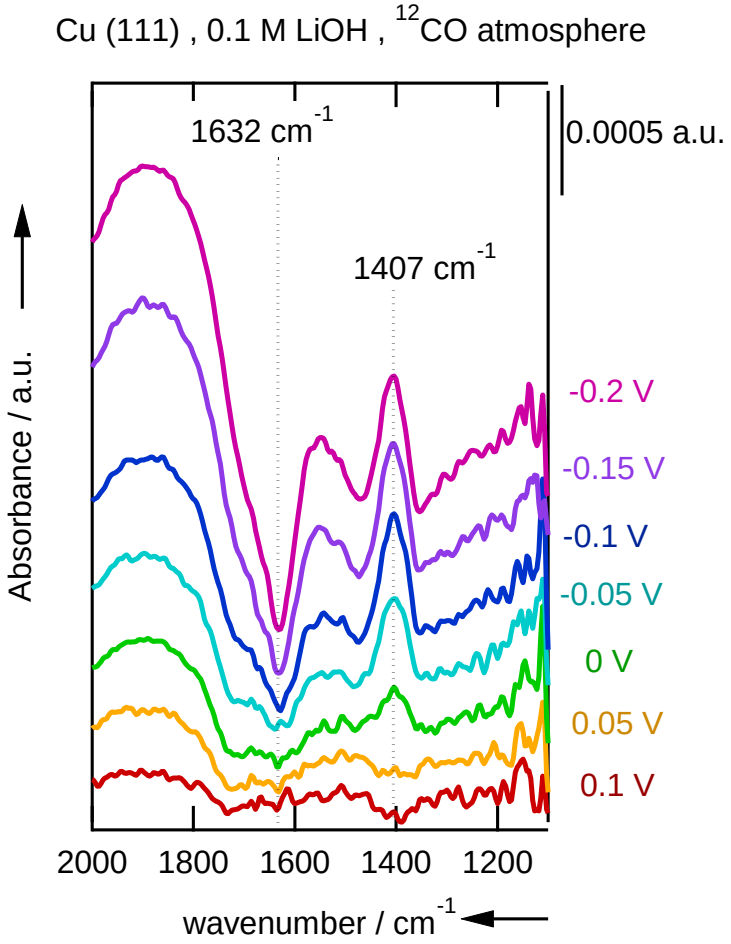

Figure AIII.1: Potential-dependent absorbance spectra for Cu(111) in the presence of CO in a 0.1 M LiOH solution. Reference spectrum recorded at +0.1 V vs. RHE. Highlighted bands and their correspondent frequency are indicated with a vertical line at 1407 cm-1 for ^{12}C-OH stretching and 1632 cm^{-1} for O-H bending.

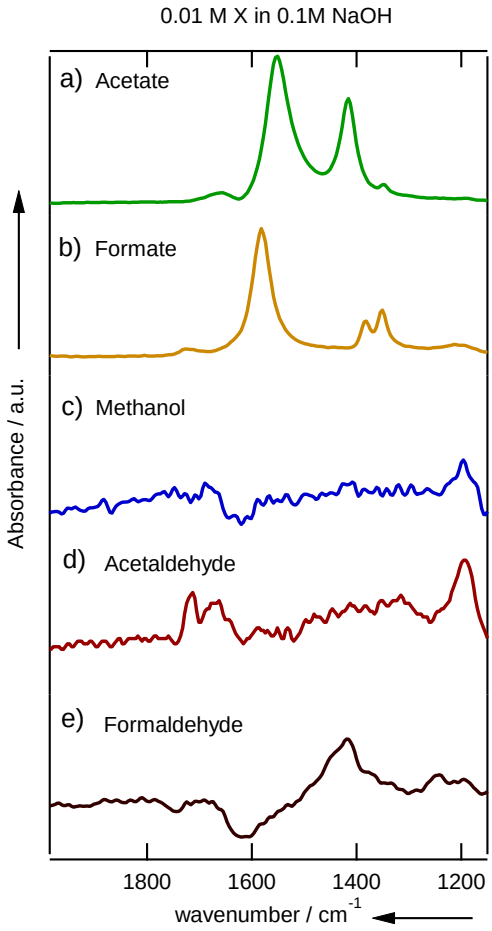

Figure AIII.2: Transmission spectra of 0.01 M of: a) acetate, b) formate, c) methanol, d) acetaldehyde, and e) formaldehyde in 0.1 M NaOH solution.

Appendix IV

Supporting information to chapter 5

IV.1 OLEMS measurements

IV.1.1 Hydrogen evolution reaction

Figure AIV.1 show the mass fragment m/z = 2 associated with the formation of H_2 from the competitive hydrogen evolution reaction (HER) during CO reduction on Cu(100), Cu(111) and polycrystalline Cu. On all copper surfaces, hydrogen evolution starts at ca. -0.4 V for all different cations except Cs^+, for which it starts at slightly less negative potentials. The amount of hydrogen produced as well as its formation rate increases with the size of the cation in the electrolyte for every copper surface

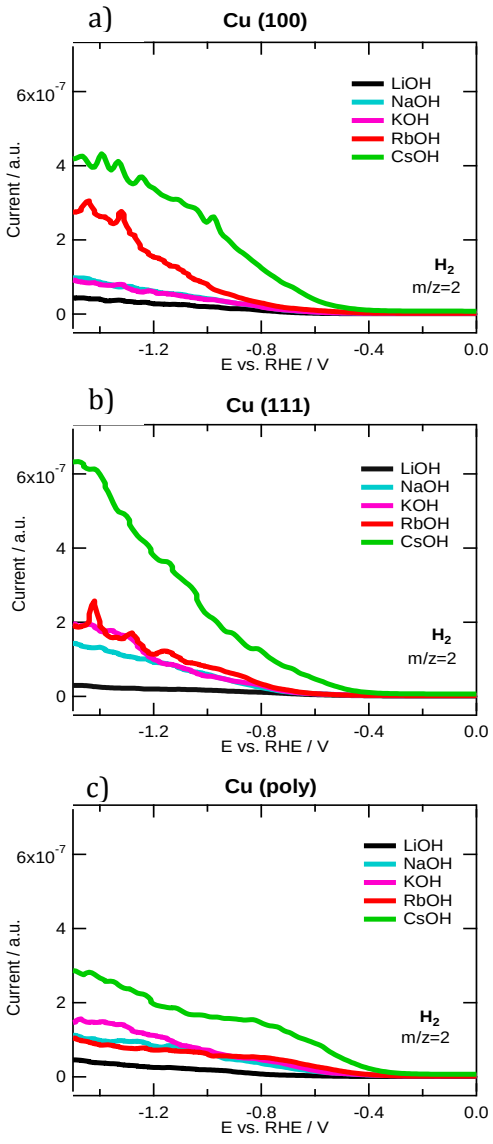

Figure AIV.1: OLEMS mass fragment m/z= associated with the formation of H_2 during CO reduction on a) Cu(100) , b) Cu(111) and c) polycrystalline Cu for different 0.1 M alkaline hydroxide solutions.

IV.1.1 Cation effect for ethylene selectivity

Figure AIV.2 illustrates the cation effect on the selectivity of ethylene versus methane on Cu(100) electrodes during CO reduction. The values in Figure AIV.2 have been extracted from Figure 5.1 for a clearer representation of the cation effect for ethylene selectivity.

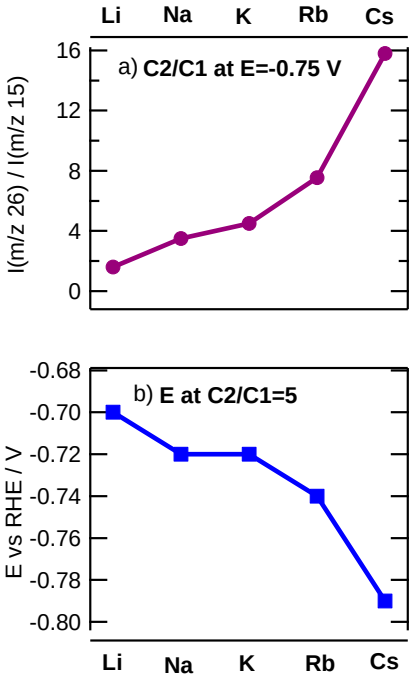

Figure AIV.2: a) ratio ethylene/methane at a representative potential of -0.75 V vs RHE for different alkali cations. b) potential for which a fixed value of 5 for the ratio ethylene/methane is obtained for different alkali cations.

Figure AIV.2a shows the ratio C_2/C_1 at a representative potential of -0.75 V vs RHE for different alkaline cations. Figure AIV.2b shows the potential for which a fixed value of 5 for the ratio ethylene/methane is obtained for the different alkaline cations. The values of the

ethylene/methane ratio at -0.75 V show a clear effect of the cation towards ethylene formation that monotonically follows the cation sizes. In addition, the potentials for wich a fixed value of 5 for the ratio ethylene/methane show that larger cations can maintain the same selectivity for ethylene at more negative potentials compared to smaller cations, suggesting that the selectivity for ethylene is enhanced in a larger potential range when larger cations are used.

IV.2 HPLC measurements

During CO reduction on polycrystalline copper, the minor liquid products formed were collected and analyzed by High- Performance Liquid Chromatography (HPLC).

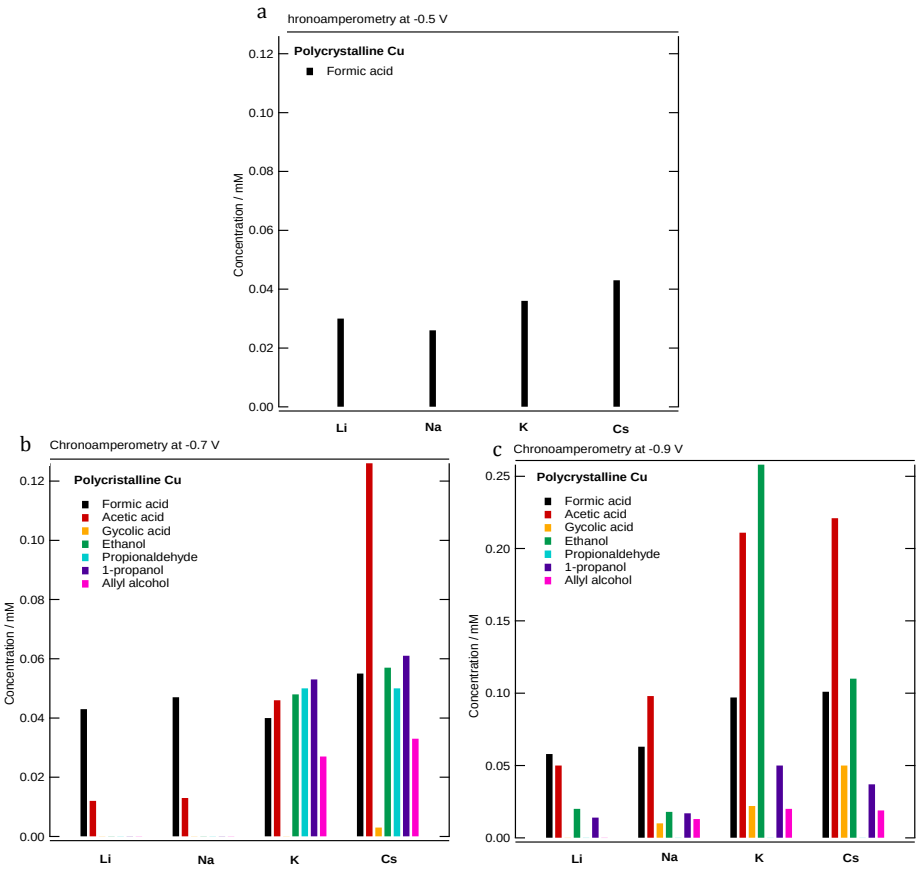

Figure AIV.3: Concentration analyzed with HPLC of different liquid products obtained during the reduction of CO after 2h of electrolysis at a) -0.5 V b) -0.7 V and c) -0.9 V on polycrystalline Cu with 0.1 M solutions of alkaline hydroxides.

Chronoamperometry experiments were carried out at three different potentials: -0.5, -0.7 and -0.9 V, with different alkaline hydroxides as electrolytes. The results are summarize in Figure AIV.2. Experiments with RbOH showed an anomalously low amount of product formation, which we ascribe to the combination of low purity and long experimentation time. Therefore, data obtained with Rb cations are not included in the results described below.

When chronoamperometry experiments were performed at -0.5 V vs RHE for 2 h (See Figure AIV.3a), the only product observed was formic acid. The concentration of this acid does not greatly change along with the cation in solution, being the concentration in the range 0.025 – 0.043 mM. Note that the formation of formic acid has been never reported as a CO reduction product. We attribute its formation here to the Cannizzaro reaction, a base-catalyzed aldehyde disproportionation resulting in the formation of the corresponding acid and alcohol. In this specific case, the formaldehyde formed during CO reduction disproportionates into methanol and formic acid. We recently pointed out the importance of this reaction[149], as it explains the concomitant formation of acids and alcohols observed during CO_2 reduction as a result of a local pH increase due to OH^- generation from the simultaneous hydrogen evolution reaction. Formate might as well be produced after *CO is hydrogenated to *CHO, and *CHO combines with OH^- according to Zheng et al. [171]

At more negative potentials (-0.7 V and -0.9 V), we observed more significant differences in terms of product distribution and concentration. The products obtained were: formic acid as C_1 product; acetic acid, glycolic acid, ethylene glycol and ethanol as C_2 products; propionaldehyde, 1-propanol and allyl alcohol as C_3 products. The C_2 and C_3 products obtained during CO reduction have been reported previously[50, 61].

At -0.7 V, formic acid is formed on all electrolytes with slight differences in concentration. However, the concentration of acetic acid, increases

with the cation size. Ethanol, propionaldehyde, 1-propanol and allyl alcohol were only observed when K^+ and Cs^+ were present in the electrolyte, with slightly higher concentrations observed for the latter. In addition, with Cs^+ a small amount of glycolic acid was produced. Ethylene glycol was also detected in KOH and CsOH, although an accurate quantification was not possible due to an overlap with the intense peak of acetic acid.

During CO reduction at more negative potentials (-0.9 V), higher concentrations of products were generally obtained. Formic acid and acetic acid were formed for all cations, with their concentrations increasing with the cation size. Ethanol and 1-propanol were also detected for every cation with the highest concentration corresponding to K^+. Small amounts of allyl alcohol were detected for Na^+, K^+ and Cs^+, without significant differences in concentration. Glycolic acid was also observed for Na^+, K^+ and Cs^+, with a clearer trend regarding the size of the cation. Ethylene glycol was detected with K^+ and Cs^+, but a clear quantification was not possible. In general, larger cations (Cs^+) promote CO reduction to C_2 species compared to small cations (Li^+ and Na^+), in agreement with the results by Hori et al[65].

IV.3 ^{1}H-NMR

The samples collected after 2h of CO reduction by chronoamperometry at -0.9 V vs. RHE in 0.1 M NaOH, KOH and CsOH solutions were analyzed by ^{1}H-NMR. The ^{1}H-NMR spectra are shown in Figure AIV.4.

Solvent supression was employed to reduce the size of the peak corresponding to water in order to magnify the peaks corresponding to CO reduction products. The product distribution obtained is similar, regardless of the cation size, although differences in the intensity of the peaks were observed.

The products observed were formic acid, acetic acid, ethylene glycol, glycolic acid, ethanol and 1-propanol, in agreement with the products

observed with HPLC. In addition, methanol was also observed as a CO reduction product for all three electrolytes analyzed. The detection of methanol by HPLC analysis was not possible due to the overlap of the corresponding peak with the peaks of the eluent. The amount of these reduction products was higher for CsOH and KOH, compared to NaOH, although an accurate quantification was not made.

Table AIV.1 shows an overview of the products detected by ^{1}H-NMR for the electrolysis experiments performed at -0.9 V vs. RHE in NaOH, KOH and CsOH 0.1 M solutions.

Table AIV.1: 1H-NMR chemical shift for the products detected after reduction of CO at -0.9 V vs. RHE in 0.1 M NaOH, KOH and CsOH solutions.

Compound	**Proton**	**Nb H**	**Mult.**	**Delta / ppm (Na^+)**	**Delta / ppm (K^+)**	**Delta / ppm (Cs^+)**
Formic acid	-H	1	s	8.376	8.367	8.359
Acetic acid	$-CH_3$	3	s	2.206	2.196	2.184
Ethylene glycol	$-CH_2-$	4	t	3.484	3.470	3.462
Glycolic acid	$-CH_2-$	2	s	3.869	3.858	3.845
Methanol	$-CH_3$	3	s	3.278	3.267	3.255
Ethanol	$-CH_2-$	2	q	3.587	3.566	3.558
	$-CH_3$	3	t	1.105	1.104	1.090
1-propanol	$-CH_3$	3	t	0.816	0.806	0.807
	$-CH_2-$	2	qt	1.105	1.098	1.095
	$-CH_2-$	2	t	3.587	3.56	3.473

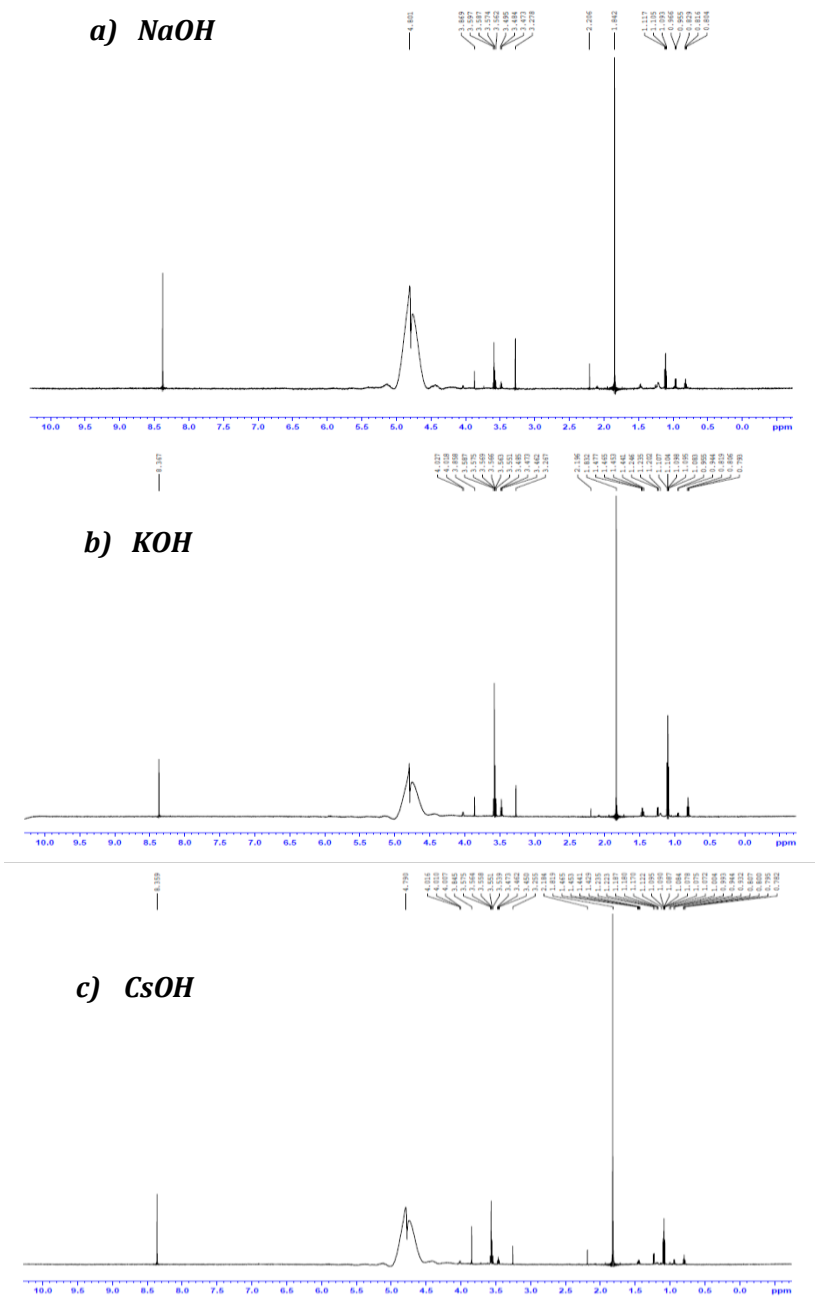

Figure AIV.4: ^{1}H-NMR spectra of the samples obtained during CO reduction on polycrystalline copper after 2h of chronoamperometry at -0.9 V vs RHE in a) NaOH, b) KOH and c) CsOH 0.1 M solutions.

IV. 4 Mechanistic implications

During the electroreduction of CO, a relation between the formation of ethylene and methane was noted: an increase in m/z = 15 (corresponding to methane) occurs when m/z = 26 (corresponding to ethylene) starts to decay. Figure AIV.5 shows the relation between these two mass fragments for Cu(111) and Cu(polycrystalline) in different alkaline hydroxide solutions, which complement Figure 5.4 in chapter 5.

The possibility that methane formation be the result of ethylene reduction has been tested. Figure AIV.6 shows the reduction of ethylene on Cu(100) in 0.1 M CsOH solution. When ethylene is reduced, only the formation of hydrogen from the competitive hydrogen evolution reaction (HER) was observed. The absence of methane formation rules out the possibility that the relation observed between methane and ethylene is due to methane production as a following step in the C_2 pathway. It is important to mention that ethane was not detected during the reduction of ethylene, either.

The decay in m/z = 26 during CO reduction due to the reduction of ethylene has also been considered. The experiments show that ethylene reduction starts at ca. -0.4 V achieving its maximum reduction current at ca. -0.6 V vs RHE, and the decay of m/z = 26 during the reduction of CO occurs at ca. -0.7 V. Thus, the possibility of the decay of the ethylene signal due to its reduction has also been ruled out. Hence, we propose that the C_2 pathway gets blocked by the enhancement of the C_1 pathway and discard the hypothesis that C_2 products are transformed to produce C_1 species.

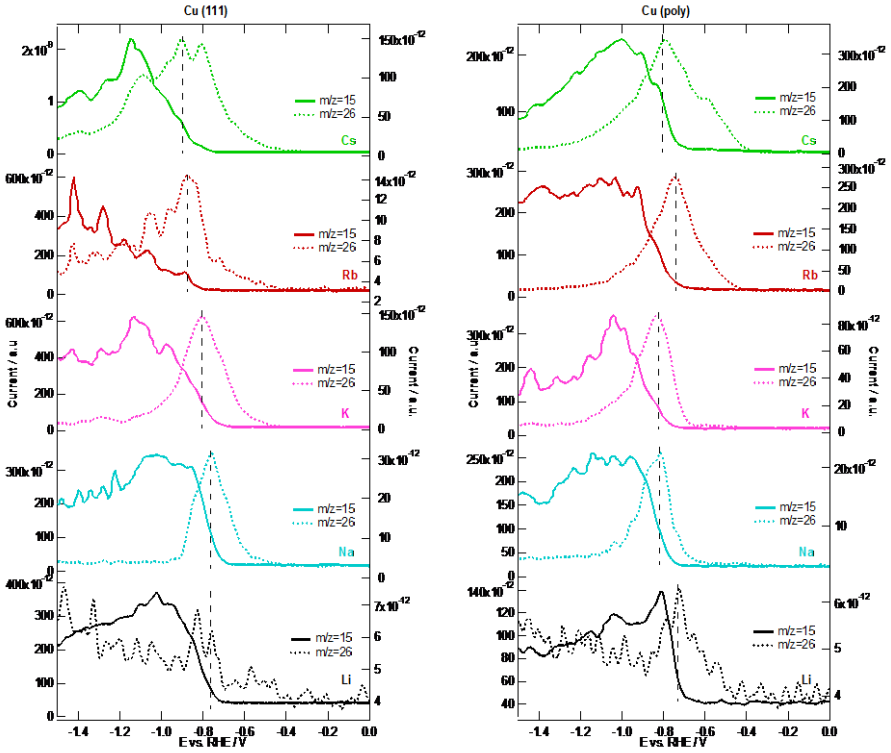

Figure AIV.5: OLEMS mass fragments associated with the reduction products formed during CO reduction on Cu(111) (left panel) in different 0.1 M alkaline hydroxide solutions. Dashed lines correspond to m/z = 26 associated with the formation of ethylene, plotted against the right axis. Full lines correspond to m/z = 15 associated with the formation of methane, plotted against the left axis.

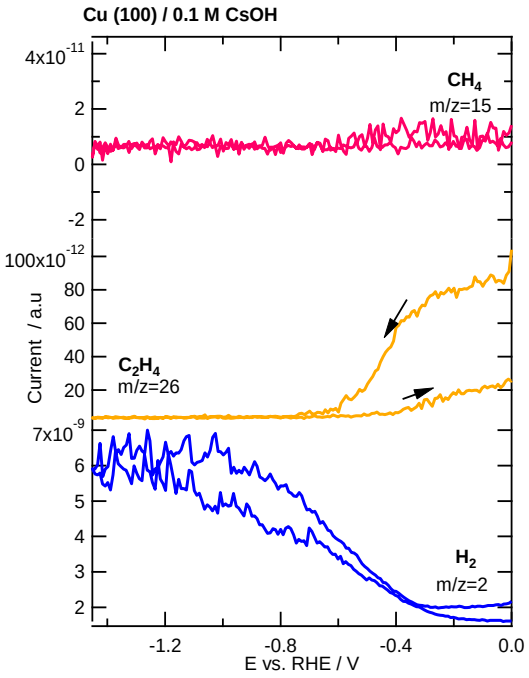

Figure AIV.6: OLEMS mass fragments associated with the reduction of ethylene on Cu(100) in 0.1 M CsOH solution. The bottom panel displays m/z = 2 associated with the formation of H2, the middle panel displays m/z = 26 associated with the reduction of C2H4 and the top panel displays m/z = 15 associated with CH4.

The onset potential for the formation of methane and ethylene during the reduction of CO is displayed in figure AIV.7. The onset potential for ethylene formation depends on the facet, being lower for copper single crystals than for polycrystalline copper. In addition, the onset potential for ethylene is not affected by the cation size when CO reduction is performed on copper single crystals, whereas on polycrystalline copper the onset potential depends on the cation, being -0.6 V for Li^+ and Na^+, -0.4 V for K^+ and -0.35 V for Rb^+ and Cs^+. On the other hand, the onset potential for methane formation is independent of both cation nature and surface structure.

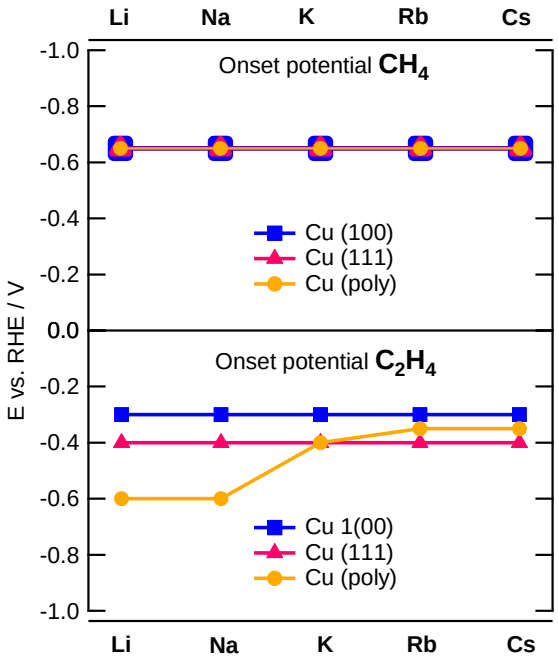

Figure AIV.7: Onset potential for the formation of methane (top panel) and ethylene (bottom panel) dependent on the cation nature and surface structure.

IV.5 Electrode surface characterization

The structure of copper electrodes is a key factor in tuning the selectivity of CO electroreduction.[64, 144] Therefore, cyclic voltammetry before and after the reduction of CO (Figure AIV.8) has been carried out in order to determine the initial state of the electrode surface and to assess its change after CO reduction.

Prior to CO reduction, the voltammograms exhibit the characteristic peaks according to the specific copper surface, in agreement with the study of Schouten et al.[91] However, the state of the electrode surface

at the end of the experiments displays some differences with respect to the initial state. . While the surfaces of Cu(100) and Cu(poly) electrodes remain relatively unchanged, Cu(111) underwent major modifications. Thus, the variation in product distribution is merely due to the nature of the cation in solution and structural factors must not be considered. On Cu(100) OH^- adsorption/desorption peaks at -0.15 V are present before and after the experiment. However, the OH^- adsorption/desorption peaks on Cu(111) decrease in current intensity after the experiment. In addition, a new irreversible anodic peak appears at +0.35 V, suggesting that the well-defined (111) arrangement has been partially lost at the end of the OLEMS experiments. This new anodic peak might be due to specific cation adsorption or to OH^- adsorption on a reconstructed surface.

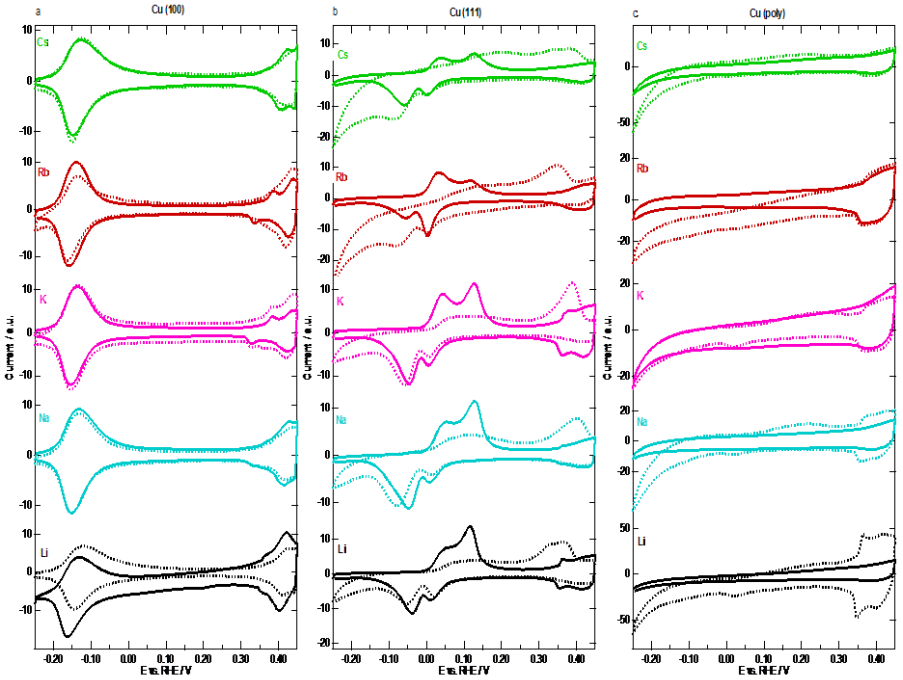

Figure AIV.8: Cyclic voltammetry characterization of a) Cu(100), b) Cu(111) and c) Cu(poly) in different 0.1 M alkaline hydroxide solutions before OLEMS experiments (full lines) and after OLEMS experiments (dashed lines).

First, according to DFT calculations in which solvation effects are considered, the specific adsorption of alkaline cations on fcc (111) transition metals occurs in the same potential range of HER[172]. Secondly, Jović et al. reported the slow Cu(111) surface reconstruction induced by adsorption/desorption of OH^-, when the potential is scanned between -0.25 V and +0.45 V vs. RHE[173]. Both processes might give a possible explanation for the modification of the Cu(111) surface.

IV.6 Computational details

Cu(100) was modeled with (3×2) slabs that contained four atomic layers. For such slabs, we sampled the Brillouin zones with 6×8×1 Monkhorst-Pack grids.[115]. The geometry optimizations were carried out using a plane-wave cut-off of 450 eV, employing the conjugate-gradient scheme until the maximum force on any atom was below 0.05 eV $Å^{-1}$, and allowing the two topmost layers and the adsorbates to relax in all directions, while the 2 bottommost layers were frozen at the optimized bulk distances. The separation between periodical images was more than 16 Å in the z direction and dipole corrections were also applied. The Fermi level in the calculations was smeared using the Methfessel-Paxton method[116] with an electronic temperature of 0.2 eV, and all energies were extrapolated to T = 0 K.

The chemical potential of protons and electrons was calculated from that of H_2(g) using the computational hydrogen electrode[121]. The free energies of the species were calculated as: $G = E_{DFT} + ZPE - TS + E_{solvation}$, where E_{DFT} is the total energy calculated in the manner described before, *ZPE* is the zero-point energy calculated through the harmonic oscillator approximation, and *TS* (with T = 298.15 K) is the total entropy correction for H_2(g) and H_2O(l), whereas it corresponds to the vibrational entropy part for the adsorbed species. We applied the solvation corrections ($E_{solvation}$) reported before for *CO (-0.1 eV/CO)[57], *OCCO (-0.3 eV/*OCCO) and *OCCOH (-0.48 eV/*OCCOH)[53] and included

explicit water in the calculations to solvate only the alkaline cations. Given the known problems of PBE for the description of CO(g)[57], we corrected its total energy by -0.24 eV as described elsewhere[53].

Figure AIV.9 contains the adsorption configurations of 2*CO, $*C_2O_2$ and $*C_2O_2H$ on Cu(100) in vacuum and in presence of the alkaline cations Li^+, Na^+ and Cs^+. Only in the case of Li^+, the calculations included one explicit water molecule, as the adsorption energy of H_2O over adsorbed Li, Na and Cs was -0.32, 0.04, and 0.19 eV, respectively.

This different solvation upon adsorption reflects the fact that in solution, the number of water molecules in the first solvation shell decrease as a function of the cation size, so that Li^+, Na^+, Cs^+ are surrounded by ~5, 3-4 and 2 H_2O molecules, respectively[174]. However, the adsorption energetics in presence of the cations are rather similar in presence and absence of water, as shown in Table AIV.2.

Table AIV.2: Energetics of adsorption on Cu(100) of two CO molecules (2*CO), their dimer ($*C_2O_2$), and hydrogenated dimer ($*C_2O_2H$). All values are in eV.

species	vacuum	Li	Li + H_2O	Na	Na + H_2O	Cs	Cs + H_2O
2*CO	-0.44	-0.77	-0.77	-0.74	-0.81	-1.04	-0.96
*C2O2	0.56	-0.51	-0.48	-0.64	-0.67	-0.76	-0.63
*C2O2H	0.44	-0.54	-0.68	-0.58	-0.72	-0.77	-0.66

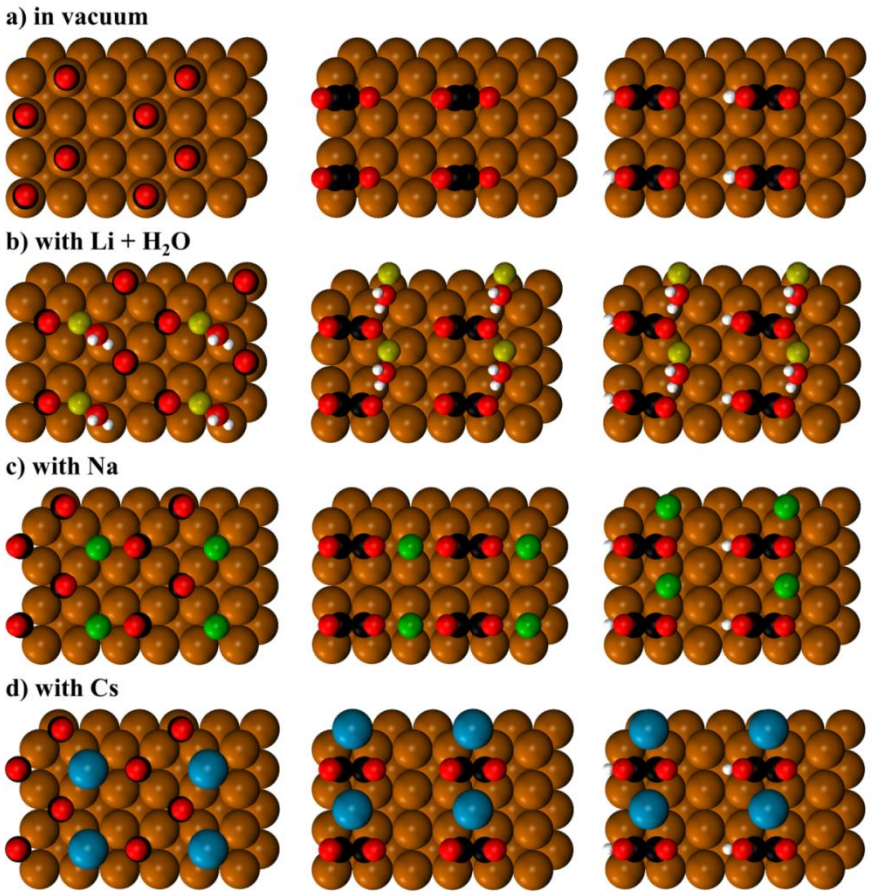

Figure AIV.9: Adsorption on Cu(100) of 2*CO (left), *C_2O_2 (center) and *C_2O_2H (right) in a) vacuum, and with b) Li, c) Na, and d) Cs. Color code: C: black, Cs: blue, Cu: orange, H: white, Li: yellow, Na: green, oxygen: red.

Essentially, the commonality between the three analyzed cations is that their effects are only present when they are relatively close to the adsorbates. The distances to the closest O atoms in the dimer vary considerably with cation: 1.88, 2.37, and 3.08 Å for Li^+, Na^+ and Cs^+, respectively.

Regarding the C_1 pathway, Figure AIV.10 contains the adsorption configurations of *CO and *CHO on Cu(100) in vacuum and in presence of the alkaline cations Li^+, Na^+ and Cs^+. Based on the adsorption energies

of water on the cations provided above, only in the case of Li^+ the calculations included one explicit water molecule. In any case, the adsorption energetics are rather similar in presence and absence of water, as shown below in Table AIV.3 for Li.

Table AIV.3: Energetics of adsorption on Cu(100) of *CO and *CHO. All values are in eV.

species	vacuum	Li	Li + H_2O	Na	Cs
*CO	-0.23	-0.60	-0.58	-0.60	-0.64
*CHO	0.51	-0.10	-0.09	-0.01	-0.10

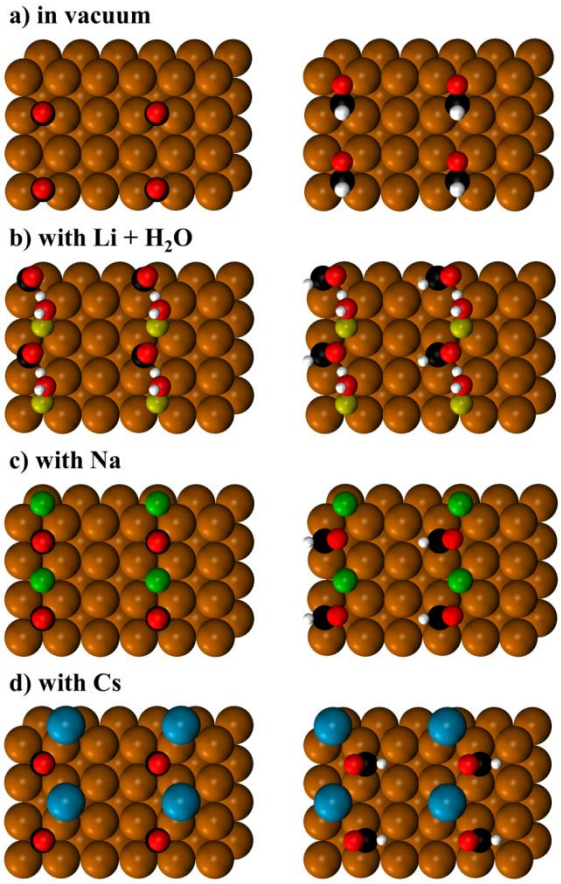

Figure AIV.10: Adsorption configurations on Cu(100) of *CO (left) and *CHO (right) in: a) vacuum, and with b) Li, c) Na, and d) Cs. Color code: C: black, Cs: blue, Cu: orange, H: white, Li: yellow, Na: green, oxygen: red

Finally, in Figures AIV.11 (C_1 pathway) and AIV.12 (C_2 pathway) we use the results in Tables AIV.2 and AIV.3 to calculate the energetics of CO adsorption, dimerization and protonation in vacuum and in presence of the cations. Note that the average values of Figures AIV.10 and AIV.11 were used to build Figure 5.3 in chapter 5.

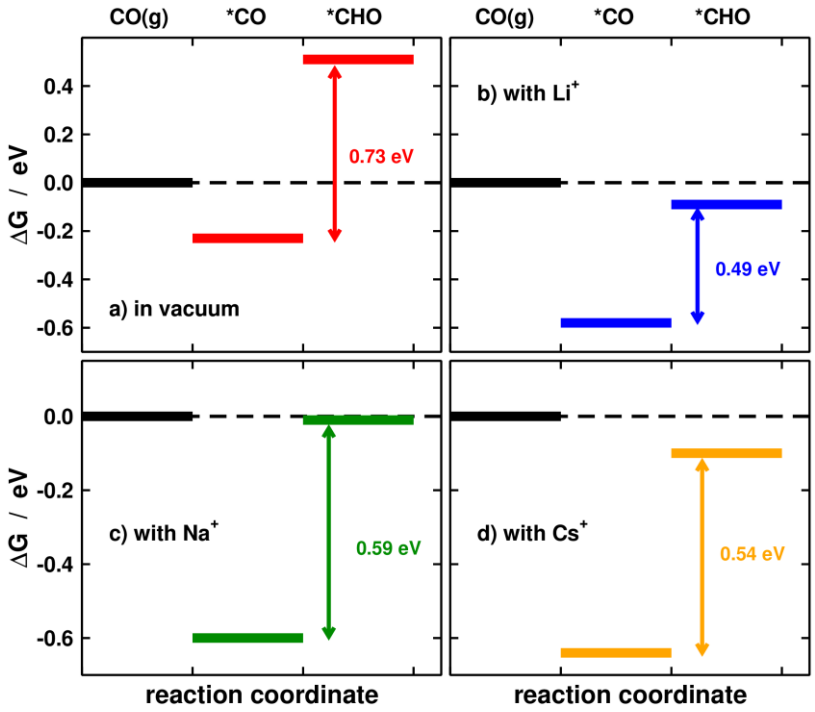

Figure AIV.11: Energetics of the first electrochemical step of CO reduction for the C_1 pathway on Cu(100) at 0 V vs RHE. a) In vacuum, and with b) Li, c) Na and d) Cs.

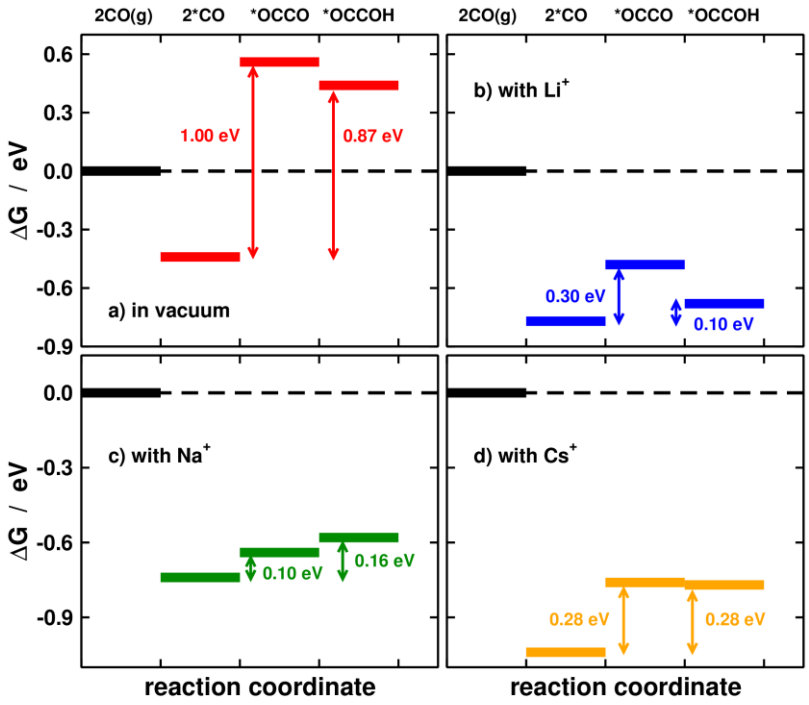

Figure AIV.12: Energetics of the first electrochemical step of CO reduction for the C_2 pathway on Cu(100) at 0 V vs RHE. a) In vacuum, and with b) Li, c) Na and d) Cs.

IV.7 Exclusion of the formation of oxalates

We have collected the solubility of some alkaline oxalates in Table AIV.4. Lithium oxalate has a solubility in water at 20 ºC of 80 g/l. On the other hand, the concentration of our hydroxides was 0.1 M. If all of the Li ions reacted to form $Li_2C_2O_4$, then 5.1 g/l would be formed. This means that all lithium oxalate that might be formed would be readily dissolved in water. Therefore, we do not expect any salt deposition during our experiments, which is corroborated by the identical cyclic voltammograms before and after electrolysis experiments.

Furthermore, we had a look at the spectra of hydrogen oxalate compounds[175] and noticed that it present a band at 1195 cm^{-1}. However, these compounds also present a prominent band at 1440 cm^{-1} corresponding to C-O stretching and a band at 1737 cm^{-1} that corresponds to C=O stretching[175]. The absence of the latter two bands in the spectra recorded during CO reduction makes it possible to rule out the formation of lithium salts of hydrogen oxalate.

We would also like to annotate that (i) we did not detect any carbonate (CO_3^{2-}) in our experiments, and (ii) oxalate ($C_2O_4^{2-}$) is a negatively charged dimer of CO_2. Taking into account that all our experiments focused on CO reduction and that carbonate was not observed, any CO-associated dimer should only have 1 or maximum 2 oxygen atoms in its structure. Therefore, if oxalate were detected from CO reduction experiments, it would counterintuitively imply that CO is first oxidized and then subsequently reduced to ethylene. Note as well that if oxalate formed from dimerization of hydrolyzed *CO, its formation rate would be slow[171] and would not account for the significant amounts of ethylene observed.

For all those reasons, we believe that oxalate is not responsible for the two bands that we attribute to the hydrogenated dimer.

Table AIV.4: Solubility in g/100 ml of several alkali oxalates

Alkali oxalate	Solubility in g/100 ml
Li	8
Na	3.7
K	36.4
Cs	313

Appendix V

Supporting information to chapter 6

V.1 Results

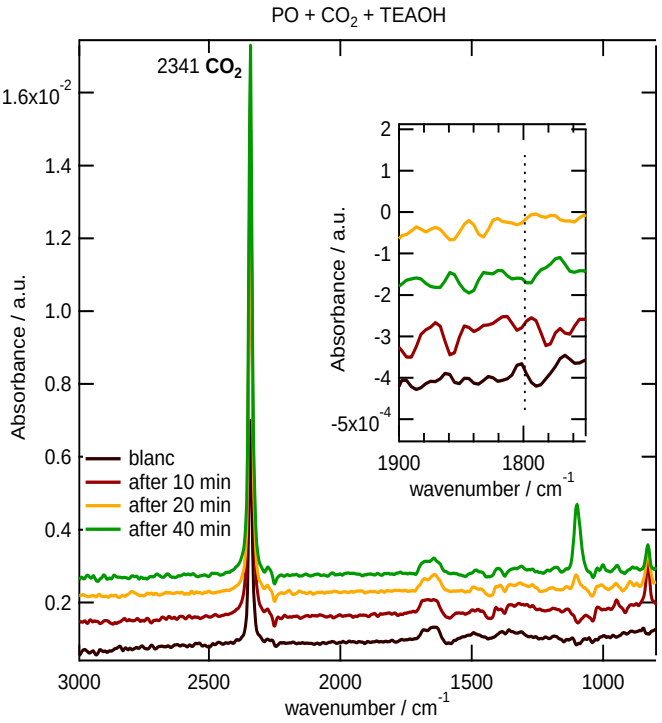

Figure AV.1: Time dependent absorbance spectra of a solution containing 0.1 M of propylene oxide, saturated carbon dioxide atmosphere in a 0.1M $TEAClO_4$ in acetonitrile solution in the absence of TEAOH (black) and in the presence of 1M TEAOH after 10 minutes (red), 20 minutes (yellow) and 40 minutes (green). The insert displays the zoom-in of the region between 1900 - 1750 cm^{-1}

Figure AV.1 shows the time dependent absorbance spectra of propylene oxide and CO_2 in the presence of a strong base (TEAOH) in a 0.1 M $TEAClO_4$ in acetonitrile solution. The spectra were recorded in order to ensure that the formation of propylene carbonate from propylene oxide and CO2 is an electrochemical process and not a chemical synthesis catalyzed by the presence of OH- which can be formed during water reduction. The spectra show an intense band at 2341 cm^{-1} corresponding to C=O stretching from CO_2 in solution. Less intense bands at 1670 cm^{-1} corresponding to decomposition products from the acetonitrile are also observed. However, the absence of a band at 1800 cm^{-1} that would correspond to propylene carbonate, supports the electrochemical nature of the synthesis of propylene carbonate instead of a chemical reaction catalyzed by OH^-, in accordance with the results observed by Yang et al.[78]